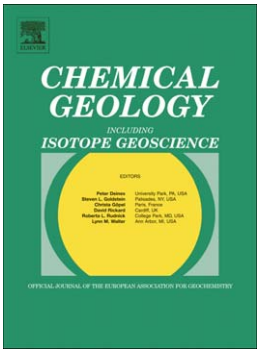

Carbonate recrystallisation and organic matter maturation in heat-affected sediments from the Shaban Deep, Red Sea

Reiner Botz, Mark Schmidt, Jolanta Kus, Christian Ostertag-Henning, Axel Ehrhardt, Nazli Olgun, Dieter Garbe-Schönberg, Jan Scholten

PII: S0009-2541(10)00396-7
DOI: doi: 10.1016/j.chemgeo.2010.11.003
Reference: CHEMGE 16079

To appear in: *Chemical Geology*

Received date: 25 December 2009
Revised date: 21 September 2010
Accepted date: 2 November 2010

Please cite this article as: Botz, Reiner, Schmidt, Mark, Kus, Jolanta, Ostertag-Henning, Christian, Ehrhardt, Axel, Olgun, Nazli, Garbe-Schönberg, Dieter, Scholten, Jan, Carbonate recrystallisation and organic matter maturation in heat-affected sediments from the Shaban Deep, Red Sea, *Chemical Geology* (2010), doi: 10.1016/j.chemgeo.2010.11.003

Carbonate recrystallisation and organic matter maturation in heat-affected sediments from the Shaban Deep, Red Sea

Reiner Botz[a,*], Mark Schmidt[b], Jolanta Kus[c], Christian Ostertag-Henning[c], Axel Ehrhardt[c], Nazli Olgun[b], Dieter Garbe-Schönberg[a], Jan Scholten[d].

[a] Institute of Geosciences, Ludewig-Meyn-Str. 10, 24118 Kiel, Germany
[b] Leibniz-Institute for Marine Sciences, IFM-GEOMAR, Wischhofstr. 1-3, 24148 Kiel, Germany
[c] Federal Institute for Geosciences and Natural Resources, Stilleweg 2, D-30655 Hannover, Germany
[d] International Atomic Energy Agency, Marine Environment Laboratories (IAEA-MEL), 98000 Monaco

Abstract

Parasound profiles across the Shaban Deep in the Red Sea indicate turbiditic transport of surface sediments from the topographic hight (basalt ridge) into the interior of the deep. This is supported by petrographical and (isotope-) geochemical evidence in the East Basin of the Shaban Deep where the presence of variable mixtures of authochtonous and allochthonous sediment compounds had been found.

The uppermost 170 cm of both sediment cores 17008-1 and 17009-3 reveal "normal" stable oxygen isotope values for the planktonic foraminifera G. *ruber* near -1 ‰ which is indicative for carbonate formation in Red Sea surface water around 27°C. However, below 182 cm in core 17008-1 highly variable $\delta^{18}O$ values for G. *ruber* between 0.26 and -10.68 ‰ occur which are not the result of temperature-controlled oxygen isotope fractionation between foraminiferal carbonate and Red Sea surface water. The lowest $\delta^{18}O$ values of -10.68 ‰ measured for highly-altered foraminifera shells suggests carbonate precipitation higher than 90°C.

Organic petrographical observations show a great diversity of marine-derived macerals and terrigenous organic particles. Based on petrographical investigations sediment core 17008-1 can be subdivided in intervals predominantly of authochtonous character (i.e. 1, 3, 5

corresponding to core depths 0-170 cm, 370-415 cm, 69-136 cm), and allochthonous/thermally altered character (e.g. 2, 4 corresponding to core depths 189-353 cm, 515-671 cm). Allochthonous/thermally altered material displays a wide to an extremely wide range of maturities (0.38-1.42 % R_r) and also natural coke particles were found.

Similarily, the organic geochemical and pyrolysis data indicate the predominance of well-preserved, immature algal and bacterial remains with a minor contribution of land plant material. Sediments below 170 cm (core 17008-1) contain contributions of re-sedimented pre-heated material most likely from the area of the basaltic ridge. This is documented by individual coke particles reduced hydrogen indices and elevated T_{max} values up to 440°C.

An "oil-type" contribution (evidenced by mature biomarkers, hopene/hopane ratios, elevated background fluorescence, n-alkane distribution) is also present in the sediments which most likely originated at greater depth and impregnated the surface sediments.

The heat source responsible for recrystallisation of foraminiferal carbonate and maturation of organic particles in Shaban Deep sediments most likely is attributed to modern basalt extrusions which now separate the Shaban Deep subbasins.

Keywords: Red Sea, carbonate diagenesis, sediments, turbidite, organic matter maturation

* Corresponding author. Email address: rbotz@gpi.uni-kiel.de (R. Botz)

1. Introduction

1.1 Tectonic setting

The Red Sea is part of the African-Arabian rift system. The basin is near 2000 km long and 230 km wide (Fig. 1a). Here a young oceanic basin is forming. Mature spreading centres exist in the central part of the Red Sea (Altherr et al., 1988) but it is unclear whether the nature of Red Sea mantle ascent is passive (Bonatti, 1985) or active (Camp and Roobol, 1992). Late stage continental rifting occurs north of 23°30`N (Cochran, 1983; Martinez and Cochran, 1988). Further south, between 20° and 23°30`N, a transition zone exists. The zone of active seafloor spreading between 15° and 20°N is characterised by the formation of oceanic crust of MORB composition since at least 3 Ma (Altherr et al., 1988; Eissen et al., 1989). The structure of the crust of the northern Red Sea basin is an ongoing matter of debate but it appears that much is underlain by thinned continental crust and mantle cut by numerous intrusions (Martinez and Cochran, 1988; Voggenreiter et al., 1988).

1.2 Hydrography

Water exchange between the Red Sea and the open ocean occurs across the shallow (137 m, Werner & Lange, 1975) sill of Bab el Mandeb and through a narrow channel close to Perim Island (Morcos, 1970). As a result of very high evaporation rates (208 cm/year; Ahmad & Sultan, 1987) which largely exceeds water inflow by land drainage and precipitation anti-estuarine water circulation develops. More details about Red Sea water masses are presented by Siddall et al. (2004) and literature given thereunder.

The restricted nature of the Red Sea makes it very sensitive to global oceanographic changes caused by sea level variations (Siddall et al., 2003). Water exchange between the Red Sea and the open ocean was much reduced by the 120 m global sea level lowering during the last glacial maximum (Fairbanks, 1989). This caused a strong increase in sea water salinity up to 50 ‰ (Locke and Thunell, 1987; Thunell et al., 1988) which was responsible for the

extinction of planktonic foraminifera (e.g. aplanktonic intervals; Deuser et al., 1976; Almogi-Labin et al., 1991; Hemleben et al., 1996b; Fenton et al., 2000 and others).

The Red Sea has numerous large depressions near the axial rift zone (Miller et al., 1966) which are usually filled with high-salinity brines up to 26 % (Hartmann et al., 1998 a,b). The origin of the brines is thought to be the result of sub-bottom leaching of Miocene evaporites (Manheim, 1974). Moreover, these deeps may contain metalliferous sediments which also indicates that they are part of hydrothermal systems (Bäcker et al., 1975; Zierenberg and Shanks, 1986; Blanc and Anschutz, 1995 and others).

1.3 The Shaban Deep

The Shaban Deep is located between 26°12`N to 26°15`N and 35°19`E to 35°24`E (Fig. 1b) within the zone of late stage continental rifting (compare above). The depression which has a size of approximately 60 km^2 was discovered during a Preussag research cruise in 1981 and studied in detail by Pautot et al. (1984). Maximum water depth of the Shaban Deep is near 1540 m, about 350 m deeper than the surrounding ocean floor. Steep slopes were observed at the southern and eastern walls (Fig. 1b). Within the Shaban Deep in the northern Red Sea basaltic crust crops out. Haase et al. (2000) found that the lavas in the Shaban Deep were of tholeiitic composition. Accordingly, magmas probably formed from an asthenospheric source distinct from the Arabian lithospheric mantle and have not assimilated crustal material. The submarine ridge at approximately 900 m water depth within the Shaban Deep represents a volcanic edifice stretching in 135° direction. It exhibits several flank cones and a surrounding plain area covered with thick layers of sediment (Haase et al., 2000). The ridge separates the Shaban Deep into four subbasins (Fig. 1b). The two larger, southern and eastern, subbasins are interconnected at 1420-1430 m water depth at the SE-end of the ridge. The brine-sea water interface occurs at a water depth near 1325 m in all subbasins. The brine has a temperature of approximately 23°C and a pH value near 6.0 (Hartmann et al., 1998a). All four

subbasins are filled with H_2S free anoxic (<0.3 mg/l dissolved oxygen; Hartmann et al., 1998a) brines with salinity values of 25.6-26.1 %, close to NaCl-saturation (Hartmann et al., 1998a).

1.4 Sediment types and carbonate diagenesis

Sediments found on the submarine ridge of the Shaban Deep are mainly biogenic with some volcanoclastic and hydrothermal sediment layers (Cocherie et al., 1994). Sediments of central parts of the Shaban Deep were sampled on the occasions of several German research cruises to the northern Red Sea (e.g. M31-2, M44-3, M52-3 between 1995 and 2002). Basically the sediment cores showed alternating light brownish to grayish or olive gray carbonaceous horizons with olive or dark gray to black laminated organic-rich (sapropels and organic oozes) layers (Stoffers et al., 1990; Hemleben et al., 1996a; Seeberg-Elverfeldt et al., 2004a,b). Sedimentation by turbidity currents is very common in the Shaban Deep and, thus, sediment dating of carbonate shells is not always reliable (Stoffers et al., 1990). However, carbon-14 dating of organic matter indicated that the cored Shaban Deep sediments are of postglacial age probably younger than 20 ka (Botz et al., 2007).

During diagenesis carbonate dissolution and/or reprecipitation is determined by the saturation state of pore water with respect to the solid phase (Morse, 2003; Funk et al., 2003). Thus, carbonate minerals in deep ocean sediments are subjected to diagenetic processes (Bathurst, 1976; Kastner, 1999 and many others). High-resolution scanning electron microscopy (SEM) showed that in particular planktonic foraminifera have high surface areas. Then even recrystallisation on a micrometer scale with good preservation of detailed shell structures is possible (Hemleben and Meischner, 1989; Pearson et al., 2001).

Calcite overgrowth of foraminifera shells often increases the $\delta^{18}O$ values (Killingley, 1983; Mulitza et al., 2004) since calcite precipitation occurs under lower (early diagenetic) temperature compared with the ocean surface water (Schrag et al., 1995). Hence, diagenetic

carbonate mineral overgrowth on planktonic shells may result in incorrect temperature determinations of paleo- sea surface water (Pearson et al., 2001).

Sediment diagenetic processes are also mirrored in the carbon isotopic composition of authigenic carbonates (Irwin et al., 1977; Pisciotto and Mahoney, 1981; Kelts and McKenzie, 1982; Botz et al., 1988). Early aerobic oxidation causes carbonate dissolution. On the other hand, subsequent anaerobic oxidation processes of organic matter in course of SO_4 – and CO_2 reduction (the latter process is responsible for the bacterial CH_4 formation) increase the alkalinity and authigenic carbonates may precipitate (Claypool and Kaplan, 1974; Berner, 1980). CO_2 produced during SO_4 reduction is isotopically light (enriched in ^{12}C) whereas CO_2 reduction produces CO_2 progressively enriched in ^{13}C (Irwin et al., 1977; Pisciotto and Mahoney, 1981; Kelts and McKenzie, 1982).

1.5 *Scientific objective*

Former work on Shaban Deep sediments (Seeberg-Elverfeldt et al., 2004a,b, 2005,) resulted in stratigraphic details with implications on paleoceanographic situations in that area. However, ^{14}C-dating and geochemical studies on organic-rich sediments in the Shaban Deep are in contrast to important results of former sediment studies (Botz et al., 2007). In order to better understand the stratigraphy of the sediments and possibly deduce paleoceanographic and paleoclimatic implications for the northern Red Sea area we analysed the stable carbon and oxygen isotopes of hand-picked foraminifera from Shaban Deep sediment cores. However, the presence of heat-altered inorganic and organic materials in young sediments of the Shaban Deep further complicate any paleoceanographic application of sediment studies. Questions on the regional heat source in the Shaban Deep,however, are of interest to numerous geoscientific researchers.

2. Methods

2.1 Sediment echosounder investigations

Several lines across the Shaban Deep were measured by the PARASOUND™ sediment echosounder (line HH02_61 in Fig. 1b) in order to resolve the surface sediments deposited southeast of the central volcanic ridge. The PARASOUND system enables high resolution profiling by using the parametric signal of 4 kHz that is the result of the interaction of two basic frequencies of 18 kHz and 22 kHz. The 4 kHz parametric signal is characterized by an emitting signal cone of only 4° which has a calculated footprint size of 7%. As a result the Parasound sediment echosounder has an excellent vertical and horizontal resolution.

2.2 Coring and sediment sample pretreatment

Sediment cores PC 17008-1 (WD 1441 m; 26°14.0'N/35°22.3'E) and PC 17009-3 (WD 1474 m; 26°13.9'N/35°22.7'E) were recovered from the Shaban Deep (Fig. 1b) by using a 12 m piston corer during METEOR 31/2 cruise (Hemleben et al., 1996a). Onboard description and photography recorded that the sediment consists mainly of alternating sapropelic and carbonate-rich mud frequently disturbed by turbiditic sand and silt layers (e.g. graded sediments; Hemleben et al., 1996a). Petroleum odor was noticed at the base of core 17008-1 (Hemleben et al., 1996a). Sapropelic sediments may be enriched with diatoms (siliceous mud) as it is described elsewhere for Shaban Deep sediments (Seeberg-Elverfeldt, 2004a,b; 2005). Sediment samples (10-30 g) were washed salt-free with distilled water, and dried at 60°C for further geochemical and isotope analyses. Foraminifera *Globigerinoides ruber* (white) were selected microscopically from 150-400 µm grain size fractions of wet sieved sediment samples.

2.3 Characterisation of sediment components

The shell texture of planktonic foraminifera *G. ruber* was documented using a scanning electron microscope (SEM) cam scan 44.

The mineralogical composition of foraminifera shells of *G. ruber* (e.g. 60 to 80 samples of bulk shell material including diagenetic mineral overgrow) was determined by XRD-analyses using a Philips PW1710 ($Co_{K\alpha}$) X-ray diffractometer.

The major element compositions of thin slights of foraminifera shells were analyzed using an electron microprobe. For preparing the EMPA samples, 15-20 *G. ruber* shells were picked and embedded in epoxy resin mounts (1" round slices). Polished and carbon coated slices were analysed by using a JEOL-JXA 8900 microprobe at the university of Kiel, equipped with 5 WDS spectrometers. An accelerating voltage of 15 kV, a probe current of 15-20 nA, and a focused beam were used for all samples.

Trace element analyses of digested sediment samples were performed with AGILENT 7500cs ICPMS. Total digestion of sediment samples was achieved by acid/pressure digestion using HNO_3/HCl/HF and $HClO_4$ according to Garbe-Schönberg (1993).

2.4 Carbon and oxygen analyses

Inorganic and organic carbon contents of pretreated sediment samples (10-15 mg) were determined with coulometry (702-LI, Ströhlein Instruments). The error in determining total inorganic carbon ($CaCO_3$) and total organic carbon (TOC) contents is ± 1-2 %.

Stable oxygen and carbon isotope analyses of foraminifera carbonate (0.05-0.1 mg) were performed using a "Carbo Kiel" online CO_2 preparation line coupled with a Finnigan MAT 252 mass spectrometer. The data are reported in permil relative to the V-PDB standard. The error is ±0.05 ‰ for carbon and ±0.08 ‰ for oxygen isotope measurements.

Absolute ^{14}C-concentrations of selected ("fresh" without mineral overgrowth; see discussion below, however) foraminifera were measured with an accelerator mass spectrometer (Tandetron 4130, High Voltage Engineering). All samples supplied the minimum carbon

weight of 1 mg C necessary for good quality dating with the AMS facility with an error less than 0.3 % (Nadeau et al., 1998). The ^{14}C-age is calculated after Stuiver and Polach, (1977).

2.5 Organic geochemical analyses

The freeze-dried sediment samples were ground in an agate mortal to less than 63 µm grain size. The total carbon, organic carbon, and sulfur content of the samples were measured using a LECO CS-200 analyzer. The type and maturity of the organic matter was analysed using RockEval pyrolysis. An aliquot of the sample was measured with a Delsi RockEval 6 instrument.

For the samples selected for molecular organic geochemical analyses an aliquot of 3 g was extracted with dichloromethane using a Dionex accelerated solvent extractor (ASE 200). Elemental sulfur was removed with activated copper. The asphaltenes were separated from the bulk extract by precipitation with petroleum ether. The remaining maltene and resins fractions were weighed and further fractionated into an aliphatic, an aromatic and a heterocompound fraction using medium-pressure chromatography with solvents of increasing polarity.

The aliphatic fraction was analysed by gas chromatography (Agilent 6890 GC-FID) using a flame ionization detector signal for quantification. The separation of the compounds was achieved with a 60 m DB-1 column (ID 0.32 mm, film thickness 0.2 µm) using a temperature program of 50°(2min)-10°/min-320°(10min) and a constant carrier gas stream of helium of 1 ml/min. Quantification was achieved for all compounds using standards of n-alkanes and their response factors.

For the identification and quantification of biomarkers gas chromatography-mass spectrometry (Agilent 6890 – Finnigan MAT 95S) was employed using both full scan and metastable reaction monitoring modes. The GC conditions were identical to those in the above mentioned GC measurements. The scan range was m/z 50-550 with a cycle time of

0.7/s and a mass resolution of 1000. The MRM measurements monitored the transitions of specific parent ions to daughter fragments of the triterpane series (m/z 191 for hopanes and m/z 217 for steranes).

2.6 Organic-petrographic investigations - Incident Light Microscopy

Dried samples were crushed to <1.00 mm, placed in a 3 cm diameter mold and vacuum-embedded using epoxy resin. After impregnation, particulate blocks were subjected to grinding and polishing according to the guidelines developed by Taylor et al. (1998). Overall up to 50 huminite/vitrinite particles were measured from each polished particulate block, in accordance with German Standard Guidelines (DIN 22020, Part 5). Leica DMRX microscope system was used for the incident and fluorescent light microscopy using x 20, x 50 and x 100 oil immersion objectives and MPV-2 photometer system. Digital images were captured using Leica DC 300 F and Image Manager (IM50) Software.

3. Results and discussion

3.1 Composition of sediments in the Shaban Deep (east basin)

Fig. 1b shows the locations of the two sediment cores under consideration. Core 17008-1 is positioned approximately 200 m west from core 17009-3 in the centre of the east subbasin of the Shaban Deep. Sediments of core 17008-1 (Fig. 2) are frequently laminated (mm to cm scale) or graded (cm to dm scale). Basically the sediments from the east subbasin are comparable to the sediments in the south basin as they are described in detail by Seeberg-Elverfeldt et al. (2004a,b) and Botz et al. (2007). In particular, graded sediments with layers of planktonic foraminifera at their base (in core 17008-1 at 0-4, 127-137, 230-255, 460-500 cm sediment depths), and features of sediment reworking (core 17008-1 at 380-400, 410-450 cm depths) suggest that also in the east basin turbidites are the major sediment transport mechanism. The turbiditic sediments within the Shaban Deep were also noted by PARASOUND

as chaotic pattern with overlap structures (Fig. 3). The analysis of all PARASOUND profiles from M52/3 (Pätzold et al., 2003) shows turbiditic sediments influencing the whole Shaban Deep basin (Ehrhardt, 2004). The alignment of the overlap structures of line HH02_61 suggests that mass transport from the central volcanic cone into the deep occurs (Fig. 3). Core location 17008-1 is approximately 300 m north to the PARASOUND track HH02_61 (Fig. 1b). The turbiditic nature of much of the sediments was also confirmed by X-ray radiographs (Olgun, 2007).

The carbonate content of sediments from core 17008-1 is variable between 0.1 and 67 % (Tab. 1; Fig. 2). Both, low carbonate values and associated high organic carbon contents up to 8.4 % are characteristic for authochtonous organic oozes and sapropels which formed within anaerobic brines of the Shaban Deep (Botz et al., 2007). Moreover, there is geochemical evidence that organic-rich sediment layers in the Shaban Deep represent times of high primary production in postglacial Red Sea surface water rather than variable stagnation conditions. In contrast, the high carbonate values in sediments of the Shaban Deep are usually attributed to turbiditic sediment input. Variable dilution of authochtonous (C-org. enriched brine-) sediment with carbonate or siliceous sediments is also responsible for variations of organic carbon contents of the sediments. For instance, the lower C-org. values of sapropels from core 17009-3 compared with sapropels from core 17008-1 (Tab. 1, Figs 2, 4) are most likely caused by dilution with carbonate material supplied by turbidites.

3.2 Stratigraphic control

Today the south and east subbasins of the Shaban Deep (Fig. 1b) contain an anaerobic brine with the same temperature and salinity (Hartmann et al., 1998a,b). Sediment core 17008-1 exhibits two distinct horizons significantly enriched in organic carbon (at 311-359 cm up to 5.3 % C-org. and 6 % C-org. at 171.5 cm; Fig. 2). Organic-rich sediments in the Shaban Deep reflect times of high organic production in Red Sea surface water (Botz et al., 2007). It is

likely that sapropels within sediments of core 17008-1 in the east basin are time-equivalent with sapropels of core 17002-2 (and also with the sapropels of core GeoB 5836-2; Seeberg Elverfeldt et al., 2005) from the south basin (Botz et al., 2007). Accordingly, absolute age-dating of sedimentary organic matter by AMS ^{14}C analyses suggests that the thick sapropel of core 17002-2 (at 309-401.5 cm core depth) formed between 11.8 and 13.6 ka during the "Younger Dryas" a time of high bioproductivity in the northern Red Sea (Legge et al., 2006). AMS ^{14}C-dating of selected foraminifera shells (*G. ruber*) with fresh appearance (see method section) from finely laminated (carbonate-poor, probably non-turbiditic) sediments in close contact with the sapropel (at 300 cm depth) and from laminated sediments just below the sapropel (at 405 cm) also indicated sediment ages between 13 ka and 10 ka for the major sapropel in core 17008-1 from the Shaban east basin (Tab. 2). Thus, the time-equivalence of the two major postglacial sapropels from cores 17002-2 and 17008-1 is reasonable to assume. Similarly, it is possible that the much thinner sapropel of core 17008-1 at 171.5 cm core depth (about 4.6 ka; Fig. 2; Tab. 2) correlates with a thin sapropel layer from the transition zone between phase I and II sediments (at 270 cm core depth, core GeoB 5836-2; Seeberg-Elverfeldt et al., 2005).

3.3 Primary control on stable carbon and oxygen isotopes of foraminifera shells

The $\delta^{13}C$ values of *G. ruber* shells from cores 17008-1 and 17009-3 are usually between 0 and 1 ‰ (Tab. 3; Fig. 5). The carbon isotope values of the shells are determined by (near-) isotope equilibrium between atmospheric CO_2 ($\delta^{13}C$ =-7 ‰; Keeling, 1958) and solid calcite. $\delta^{13}C$ values near 3 ‰ are typical for inorganic calcite as there is a 10.2 ‰ fractionation between CO_2 and carbonate at 20°C (Emrich et al., 1970). Biogenic carbonate formation includes a "vital effect" which is responsible for somewhat lower $\delta^{13}C$ values (close to 0 ‰) which may explain the observed δ-values of recent to subrecent *G. ruber* shells from core 17008-1 (at 0 to 170 cm depth) and all shells from core 17009-3.

The stable oxygen isotope compositions of the planktonic foraminifera *G. ruber* from both cores of the east basin (17008-1 and 17009-3) are shown in Fig. 6 and the data are presented in Tab. 3. Although there are a few minor excursions to more positive $\delta^{18}O$ values to 0 and 0.7 ‰ (Fig. 6; Tab. 3), recent to subrecent (at 0-170 cm core depth) *G. ruber* shells of both cores have very similar isotope values ($\delta^{18}O$ near –1‰). The oxygen isotope composition of northern Red Sea surface water is near 1.2 ‰ rel. SMOW (Ganssen and Kroon, 1991). $\delta^{18}O$ values of calcitic carbonate shells are the result of (near-isotopic equilibrium) temperature-related oxygen isotope fractionation between carbonate and sea water (Epstein et al., 1953 and others since). Assuming a mean $\delta^{18}O$ value of –1 ‰ for recent and subrecent calcite shells from cores 17008-1 and 17009-3 an isotopic carbonate formation temperature of 27°C can be calculated. This calculated carbonate formation temperature falls in the range of temperatures known for surface water of the northern Red Sea (the water temperature in the northern Red Sea during summer is on average 26°C and some 2 °C less in winter; Ganssen and Kroon, 1991). If the most positive $\delta^{18}O$ value of 1.8 ‰ would be used in the equation of Epstein et al. (1953), however, a low carbonate formation temperature of 14°C is calculated. This theoretical water temperature is not in accordance with Red Sea surface water. Hence, high

sea water salinity during low sea level stands in the Red Sea probably caused the positive $\delta^{18}O$ values of *G. ruber* shells. For instance, Hemleben et al. (1996b) measured positive $\delta^{18}O$ values up to about 2 ‰ for *G. ruber* from core Meteor 174/KL 11 (18°46.3`N; 39°19.9`E) in sediments deposited during low sea level stands (note the presence of an aplanktonic zone in Red Sea sediments due to an extreme water salinity). Hence, we can assume that postglacial sediments of the Shaban Deep contain various mixtures of *G. ruber* shells which grew during glacial and interglacial times. The glacial sediment material was probably redeposited by turbiditic activity.

3.3 Diagenetic control on foraminiferal carbonate

SEM observations of planktonic foraminifera shells in sediments of core 17008-1 from the Shaban Deep (Fig. 7) show dissolution features. On the other hand, the microfossils exhibit variable (in both thickness and surface cover) calcite overgrowth. Although not reported quantitatively microscopic observations of the sample material clearly indicate that the presence of diagenetic calcite overgrowth determines the stable isotope values of diagenetically altered *G. ruber* shells of core 17008-1 (Tab. 3, Fig. 5). One example is a negative $\delta^{18}O$ shift to -3.75 ‰ at 20 cm core depth in core 17008-1 a value significantly out of the range of $\delta^{18}O$ values found for recent foraminifera in the northern Red Sea (Ganssen and Kroon, 1991; Hemleben et al., 1996b; Arz et al., 2003; Lamy et al., 2006). Even stronger excursions towards light oxygen isotope values to –10.68 ‰ were noted in sediments of core 17008-1 between about 182 cm and 524 cm core depth (Fig. 5). The low oxygen isotope values between 182 and 524 cm are not uniform, however, as within that depth range the $\delta^{18}O$ values of *G. ruber* shells strongly vary between 0.26 ‰ and –10.68 ‰ (Fig. 6; Tab. 3). This indicates high temperatures (up to 90°C) for carbonate-(pore-)water isotope equilibrium if normal Red Sea derived pore waters with an oxygen isotope composition of +1.2 ‰ rel. SMOW is used for calculation. However, due to water-rock reactions more positive $\delta^{18}O$

values are well known for hydrothermal fluids with endmember magmatic waters having the most ^{18}O-enriched isotope value near +7‰ (Fritz & Fontes, 1980). Considering this span of very positive isotope values for the fluid the calculated temperatures of secondary carbonate formation increases up to150°C. Since the samples not only contain recrystallised carbonate but probably also original foraminifera shell material of unknown quantities the calculated isotopic temperatures between 90 and 150°C (depending on the isotope values of the fluid) represents even minimum formation temperatures. Thus, it appears reasonable to assume that the actual diagenetic calcite formation (e.g. mineral overgrowth) of sample 523 cm occurred at a significantly higher temperature than 90°C.

Note that for comparison purposes also other types of foraminifera were investigated isotopically (Fig. 6, Tab. 4). Although variable in the extent of their oxygen isotope shifts the data clearly show that also other types of planktonic foraminifera from that depth range exhibit strongly negative isotope values. Such negative oxygen isotope values are not known for living foraminifera from world's oceans and secondary ^{16}O enrichments due to recrystallisation under secondary heat influence must have occurred.

As already has been mentioned core 17008-1 contains numerous turbidites. Accordingly the foraminifera shells were sampled from turbiditic sediments. Nevertheless a theoretical possibility may exist that carbonate recrystallisation under high temperature could have occurred *in situ* within the sediments of the centre of the east basin. However, sediment heating by *in situ* hydrothermal venting in the centre of the Shaban east basin appears unlikely as indications for hydrothermal activity were not detected in that area (Hemleben et al., 1996a). Moreover, the sediment record of core 17008-1 does not show hydrothermal sediments as they were described from elsewhere in the Red Sea area (summarized by Scholten et al.; 2000). Accordingly, selected trace element concentrations of bulk samples of sediment core 17008-1 (Tab. 5) indicate no enrichment of hydrothermal elements (e.g. Li, Zn, Ba, W) relative to "normal" deep sea sediments (Fig. 8), which are composed of deep sea

carbonate, pelagic clay or mixtures of both (McLennan and Murray, 1999). However, recrystallisation of calcitic shells could have occurred in hydrothermal sediments deposited on the basaltic ridge of the Shaban basin. In order to check on this hypothesis we measured selected element concentrations along profiles across *G. ruber* shells from core 17008-1 using the electron microprobe. An example of these analyses is shown in Fig. 9. We detected neither significant enrichments nor decreasing element concentrations along profiles across individual shells. Moreover the element concentrations of recrystallised shells are comparable to those from non-recrystallised shells (Fig. 9). Note the only exception is Mn which is somewhat enriched in the recrystallised shell. This may be the result of diagenetic Mn remobilisation in sapropelic sediments and it`s reprecipitation (including diagenetic rhodocrossite formation) within certain sediment horizons of the Shaban sediments; Stoffers et al.,1990). Apart from Mn the recrystallisation of shells occurred without significant element transport reflecting a rather uniform character of the fluid during the recrystallisation process (see also discussion below).

Similar to the oxygen isotope values the somewhat lower $\delta^{13}C$ values of numerous *G. ruber* shells (Tab. 3, core 17008-1) are most likely related to the mineral overgrowth. This relative to oxygen little carbon isotope shift is explained as temperature effect. It shows that secondary calcite overgrowth incorporated the primary dissolved inorganic carbon involving no other carbon source. An exception is sample 523 cm in core 17008-1 where we measured a $\delta^{13}C$ value of -6.35 ‰ which indicates an additional organic carbon source for diagenetic calcite formation. From the presence of pyrite in the sediments (internal fillings of foraminifera and framboidal pyrite; Fig. 9) sulfate reduction likely occurred within sediments of the Shaban Deep. In accordance, sulfate reduction and ^{12}C-enriched carbonate crust formation was indicated at various depths within surface sediments of the Shaban south basin (Stoffers et al., 1990). However, only one sample at 523 cm (17008-1) core depth from the Shaban east basin revealed a comparable negative carbon isotope value. In case *in situ* sulfate

reduction would have contributed to the organic carbon content of the pore water in core 17008-1systematic $\delta^{13}C$ change with depth should be recorded in the authigenic carbonates (Irwin et al., 1977; Pisciotto and Mahoney, 1981 and others since). Thus, the occurrence of a single ^{12}C-enriched *G. ruber* sample in core 17008-1 also supports the idea of sediment redeposition rather than *in situ* carbonate precipitation. Sample 523 cm also had by far the most negative $\delta^{18}O$ value (indicating a significant heat influence during carbonate formation, see above). Thus, we may assume that mineral overgrowth on microfossils (at 523 cm in core 17008-1) incorporated organic carbon from sulfate reduction or decarboxylation reactions which probably occurred in the original sediments deposited close to the ridge basalt contact zone.

3.5 Organic Petrology

Further support for an extern sediment heating process and subsequent turbiditic transport of heat-altered material into the deep sediments comes from organic petrographical and organic geochemical investigations. Core sediment samples from the Shaban Deep contain microscopically visible and identifiable organic matter of distinct marine and terrestrial origin. Marine-derived macerals occur either as strongly fluorescing algal bodies e.g., Fig. 10-8. Terrigenous organic particles on the other hand are represented by pollen pollen e.g., Fig. 10-2 or other sporomorphs e.g., Fig. 10-12 as well as detrohuminite (e.g., Fig. 10-1), detrovitrinite (e.g., Fig. 10-4 and 10-6) as well as a variety of inertinitic macerals. Additionally a large number of the terrigeneous particles display an apparent thermal degradation, e.g., Fig. 10-3, -5. Moreover, in addition to thermal alteration observed in organic constituents also clear mineralogical changes could be detected. Samples 3,4,5,7 (Tab. 6) contain sulfides other than pyrites, partially corroded. In samples 11 and 12 (Tab. 6) oxidised framboidal pyrites were microscopically identified.

The performance of representative vitrinite reflection measurements was hindered by both, a poor surface quality as well as diminutive size of the detrohuminite/detrovitrinite particles encountered. Their microscopic surface was often characterized by dirty appearance and porous texture as seen in Fig. 10-1. Particle size in samples 5,6 and 7 (Tab. 6) was in general lower than 3-4 µm shown in Fig. 10-6. None the less, reflection measurements were performed on selected particle surfaces which were regarded as being of sufficient quality. The measured maturity of humic land derived substance ranges from peat to high volatile bituminous A coals (Tab. 6). This accords well with the respective alteration of organic fluorescence attributed to the liptinitic matter, i.e., a relative so-called “derived maturity” ranging between pale green through intensive yellow, orange, dark orange, to brown, dark brown and black shades. Similarly, in all examined intervals dispersed bituminous particles, i.e. the precursors of detrohuminite, with reflectance lower than 0.37% Rr were observed.

These particles as such do not contribute to the respective maturity of a given interval. Their lack however, as shown in sample 11 and 12, (Tab. 6) may provide an insight into diagenetic path of these botanic forerunners, i.e., caused either upon the re-sedimentation due to physical degradation or upon the previously mentioned thermal influence. Both scenarios seem to be reasonable.

Petrographic examinations revealed the occurrence of several well-defined intervals (Tab. 7) pointing towards distinct sedimentary sequences of both, predominantly authochtonous sequences (sediment intervals 1, 3, 5 in core 17008-1, Tab. 7) as well as allochthonous and of thermally altered series (sediment intervals 2 and 4 in core 17008-1, Tab. 7).

In the predominantly authochthonous intervals and in close association with representative detrohuminite/detrovitrinite populations of 0.38% Rr in interval 1, 0.55% Rr in interval 3 and 0.63% Rr in interval 5 (Tab. 7), also some reworked higher mature detrovitrinite were observed (Fig. 10-4, -6). The occurrence of higher mature dispersed organic matter in sedimentary basins is natural. These particles are thought to become additionally incorporated into the sedimentary succession via erosion of geologically speaking older successions at the time of sedimentation. Given, their comparable occurrence in both intervals 4 and 5 (Tab. 7), a common source for these intervals is to be assumed. Further, the same source is likewisely to be active prior to deposition of the sedimentary matter in interval 4 (Tab. 7) in the Shaban Deep.

In contrast, sediment intervals 2 and 4 (Tab. 7) with a predominantly allochthonous / thermally altered character display a wide to an extremely wide range of maturity distribution with huminite/vitrinite reflectance from 0.38 to 1.42% Rr. The representative measured maturity of 0.82-0.93% Rr in interval 2 and of 0.87 to 1.12% Rr in interval 4 corresponds to the derived maturity (Tab. 6). The lower reflectance are measured on lower mature detrovitrinite and detrohuminite particles. Their maturity range is comparable to that of intervals 1, 3 and 5 (Tab. 7) pointing therefore to a relatively constant source of supply in

these intervals. Furthermore, microstructural features of examined detrovitrinites point towards an apparent thermal alteration as reflected by their degraded, oxidised, corroded and partially extremely porous surfaces plus remnants and relicts as shown in Fig. 10-5.

Moreover, next to elevated maturities of about 1.0 to 1.4% Rr also natural coke particles with fine grained mosaic anisotropy were detected. Besides optical anisotropy en-countered natural coke particles display an extremely porous texture. Thermal alteration of organic matter is known to occur in many sedimentary basins with coal seams and siliciclastic sedimentary successions being invaded by a number of igneous intrusions such as dykes, sills, etc.. The heat effects are in such cases local and occur over short periods of time. Extremely high thermal influence on dispersed organic matter can be represented by natural coke particles and thermally metamorphosed organic matter (Kwiecińska and Petersen, 2004). In laboratory experiments, terrigeneously derived macerals of vitrinite and liptinite macerals display profound changes when subjected to temperature range 300-500°C (Brooks and Taylor, 1968). The product formed at 500°C is being referred to as coke with mosaic structures. It seems therefore probable that the encountered and thermally altered dispersed organic matter formed at a similar temperature range. Further, distortion of the original microstructure, i.e. formation of pores in the dispersed organic matter derived from the allochthonous intervals might be indicative of degasification of volatile matter.

The remnants and relicts resemble to a certain degree char morphology which itself is known to occur as a result of coal combustion in thermal power stations.

The occurrence of the allochthonous intervals supports a general acceptance of submarine sediment gravity flows e.g. turbidity flows in case of Newtonian flows or debris flows in case of plastic flows.

3.6 Organic geochemistry

The organic material in the uppermost sediments (-1.7 m in 17008-1, -0.7 m in 17009-3) with a TOC content of 1.5 to 1.8 % is characterized by a mixture of very well preserved, immature algal and bacterial remains with a minor, but characteristic contribution of land plant derived material for both sites. The pyrolyses results (T_{max}, HI in Tab. 8) confirm this mainly marine origin with hydrogen index values of 235-265.

A small contribution from re-sedimented organic material with higher maturities is likely because of the slightly elevated T_{max} values of 416°C and the presence of fully equilibrated homohopane isomers. But the predominance of the unsaturated biomarkers (e.g. the hopene/hopane-ratio) clearly documents the restricted importance of this component in the surficial sediment layers (Fig. 11).

Sediments deeper than 1.7 m at site 17008-1 contain larger contributions of re-sedimented material from the ridges with elevated heat flows, documented by individual coke particles, reduced hydrogen indices and elevated T_{max} values up to 440°C (Tab. 8). But in addition to this ex-situ heating of a significant proportion of the sediment a concomitant alteration of the organic matter by hot fluid flow after sedimentation is evident because of the strong reduction of the concentrations of immature biomarkers, e.g. visible in the hopene/hopane-ratio (Fig. 11). This is evident in the elevated background fluorescence of the organic matter, too (Fig. 11).

Most of the samples from this depth interval contain a significant “oil-type” contribution (clearly visible in the n-alkane distribution and mature biomarker patterns) to the extractable organic material (Fig. 12). This component might have been added during the fluid flow through the sedimentary column. The macroscopic presence of “oily material” was documented for the depth of 6.67m in the core description.

Corroborating evidence of this – perhaps much localized – fluid flow are cm-sized bleached zones, identified as “reaction zone” in the core description e.g. at 3.2 m. The coincidence of

these zones with high concentrations of biomarkers indicative of methane-oxidizing microorganisms (C40-biphytanes), for example at 1.9 and 5.2 m depth, and a mixture of very immature and mature, equilibrated biomarker isomers call for the addition of a in-situ microbial component to the organic material.

4. Conclusions

Parasound data show the surface sediments of the Shaban Deep to be largely transported by turbidites which derived from topographic heights at the edge of the deep but they also derived from top of the basaltic ridge separating the eastern and southern subbasins of the Shaban Deep.

The composite nature of the sediments is reflected in the sediment composition of the eastern subbasin of the Shaban Deep. The surface sediments within the deep are of mixed origin: authochtonous green to black-colored sediments reflect the anaerobic brine depositional environment whereas brown to gray mostly carbonate-rich sediments are allochthonous in origin and were transported by turbidites. Detailed (isotope-) geochemical investigations of inorganic and organic sediment constituents are useful when differentiating the complex nature of the sediments.

Sediment cores 17008-1 and 17009-3 from the east subbasin of the Shaban Deep were investigated in detail. Although both cores were taken very close to each other and are very similar in length they partly display very different geochemical data. Stable oxygen isotope values measured for the planktonic foraminifera *G. ruber* hand-picked from the uppermost 170 cm of sediments are similar for both cores. Here the $\delta^{18}O$ values of *G. ruber* are near -1 ‰ which reflects near isotope equilibrium for carbonate shell formation in warm (27°C) Red Sea surface waters. The $\delta^{18}O$ values of *G. ruber* from core 17009-3 fluctuate between - 1.48 and 1.64 ‰ with a slight systematic increase with depth. These values are common for planktonic foraminifera in young sediments from the Red Sea and reflect their formation

temperature and changing salinities of Red Sea surface waters. However, *G. ruber* selected from sediment core 17008-1 below 182 cm sediment depth exhibits extremely variable stable oxygen isotope values between 0.26 and -10.68 ‰. Such negative oxygen isotope values are highly unusual and are not the result of shell growth of living planktonic foraminifera in surface water of the Red Sea. SEM-observations clearly indicate that diagenetic processes and carbonate overgrowth changed the isotope values of the foraminifera shells. Based on the isotope value of -10.68 ‰ temperature of carbonate formation of 90 to 150°C (depending on a span of assumed isotope values for the fluid) is calculated. More realistic temperatures for diagenetic carbonate growth could be determined if the pure diagenetic overgrowth would be analysed. This was not possible and thus, the calculated temperature range represents a minimum temperature.

Organic petrographical observations show a great diversity of marine-derived macerals and terrigenous organic matter in surface sediments from the eastern subbasin of the Shaban Deep. According to the microscopic observations sediment core 17008-1 can be subdivided in intervals predominantly of authochtonous character (e.g., 0-170, 69-136, 370-415 cm core depth) and allochthonous/thermally-altered character (e.g., 189-353, 515-671 cm core depth). The thermally- altered allochthonous organic particles show a wide range of maturities (0.38-1.42 % Rr) and natural coke particles are found within these sediment intervals. The organic geochemical and pyrolysis data indicate a predominance of well-preserved immature algal and bacterial remains with a minor contribution of land plant material. Individual coke particles reduced hydrogen indices and elevated Tmax values up to 440°C in sediments below 170 cm of core 17008-1 are explained by the presence of re-sedimented pre-heated materials in the core. Additionally, a petroleum impregnation of the deeper sediment sequence of core 17008-1 is indicated by the strong reduction of concentrations of immature biomarkers (e.g., hopene/hopane-ratios) and elevated background fluorescence of organic matter reflecting an "oil-type" contribution (confirmed by n-alkane distribution and mature biomarker patterns).

Petrographical observations and (isotope-) geochemical data from young (to 13 ka) surface sediments of core 17008-1 indicate the presence of "normal" sediment compounds mixed with high-temperature altered sediment materials. Although the presence of turbiditic sediments is also indicated for core 17009-3 a high-temperature influence was not detected. This indicates that the source of the turbiditic materials in the basin differs between the locations.

In-situ temperatures within the Shaban East Basin are low and the trace element data do not indicate recent to subrecent hydrothermalism within that area. Moreover, the close association of low and high-temperature sediment material suggests that mixing normal low-temperature authochtonous sediment material with reworked particles is responsible. The source of the turbiditic high-temperature altered material in sediment core 17008-1 largely derived from the basaltic ridge separating the east and south basins.

The temperature and absolute age of the basaltic ridge in the Shaban Deep is very difficult to determine. However, temperature-influenced foraminifera shells from core 17008-1 are younger than approximately 13 ka which also points to a very young age of the (post) magmatic activity.

Acknowledgements

Cruise leaders Peter Stoffers and Jürgen Pätzold are acknowledged for supporting the sampling campaigns during M31/2 and 52/3, respectively. Inge Dold is acknowledged for sample preparation and coulometric measurements, and Ulrike Westernströer for help with ICPMS analyses. Peter Appel and Barbara Mader operated the electron microprobe. SEM was conducted in the laboratory of Priska Schäfer. Petra Fiedler performed XRD measurements. Nils Anders and Pieter Grootes are responsible for stable isotope and ^{14}C-measurements, respectively, at the Kiel Leibniz Laboratory. The International Atomic Energy Agency is grateful for the support provided to its Marine Laboratories by the Government of the

Principality of Monaco. Financial support was mainly given by Peter Stoffers through DFG grants STO110/39-1, and STO110/23-1.

References

Ahmad, F., Sultan, S.A.R., 1987. On the heat balance terms in the central region of the Red Sea. Deep Sea Res. 34, 1757-1760.

Almogi-Labin, A., Hemleben, C., Meischner, D., Erlenkeuser, H., 1991. Paleoenvironmental events during the last 13.000 years in the central Red Sea as recorded by pteropoda. Paleoceanography 6, 83-98.

Altherr, R., Henjes-Kunst, F., Puchelt, H., Baumann, A., 1988. Volcanic activity in the Red Sea axial trough – evidence for a large mantle diapir? Tectonophys. 150, 121-133.

Arz, H.W., Lamy, F., Pätzold, J., Müller, P.J., Prins, M., 2003. Mediterranean Moisture Source for an Early Holocene Humid Period in the Northern Red Sea. Science 300, 118-121.

Bäcker, H., Lange, K. and Richter, H., 1975. Morphologie of the Red Sea Central Graben between Subair Islands and Abul Kizaan. Geol. Jahrb. D13, pp.79.

Bathurst, R.G.C., 1976. Carbonate Sediments and their Diagenesis. Developments in Sedimentology, 12. Elsevier, New York, pp.658.

Berner, R. A., 1980. Early Diagenesis. Editor: Berner, R.A., Princeton University Press, New York, 1-241.

Blanc, G., Anschutz, P., 1995. New stratification in the hydrothermal brine system of the Atlantis II Deep, Red Sea. Geology 23, 543-546.

Bonatti, E., 1985. Punctiform initiation of seafloor spreading in the Red Sea during transition from a continental to an oceanic rift. Nature 316, 33-37.

Botz, R., Faber, E., Whiticar, M.J., Brooks, J.M., 1988. Authigenic carbonates in sediments from the Gulf of Mexico. Earth and Planetary Science Letters 88, 263-272.

Botz, R., Schmidt, M., Wehner, H., Hufnagel, H., Stoffers, P., 2007. Organic-rich sediments in brine-filled Shaban- and Kebrit deeps, northern Red Sea. Chem. Geol. 244, 520-553.

Brooks, J. D., Taylor, G. H. 1968. Chemistry and Physics of Carbon - Vol. 4. Ed. P. L. Walker Jr., Marcel Dekker Inc., New York.

Camp, V.E., Roobol, M.J., 1992. Upwelling asthenosphere beneath western Arabia and its regional implications. J. Geophys. Res. 97, 15255-15271.

Claypool, G.E., Kaplan, I.R., 1974. The origin and distribution of methane in marine sediments. In: I.R. Kaplan (Editor), Natural Gases in Marine Sediments. Plenum Press, 99-139.

Cocherie, A., Calvez, J.Y., Oudin-Dunlop, E., 1994. Hydrothermal activity as recorded by Red Sea sediments: Sr-Nd isotopes and REE signatures. Mar. Geol. 118, 291-302.

Cochran, J.R., 1983. A model for the development of the Red Sea. Bull. Amer. Assoc. Pet. Geol. 67, 41-69.

Deuser,W.G., Ross, E.H., Waterman, L.S., 1976. Glacial and pluvial periods: their relationship revealed by Pleistocene sediments of the Red Sea and Gulf of Aden. Science 191, 1168-1170.

Ehrhardt, L. A., 2004. Seismic and Hydroacoustic Studies of Surfcial Sediment Tectonics along the Northern Red Sea Rift and the Dead Sea Transform Fault. PhD thesis, Hamburg University, 127 p.

Eissen, J.-P., Juleau, T., Joron, J.-L., Duprè, B., Humler, E., Al'Mukhamedov, A., 1989. Petrology and geochemistry of basalts from the Red Sea axial rift at 18° north. J. Petrol. 30, 791-839.

Emrich, K., Ehhalt, D.J. and Vogel, J.C., 1970. Carbon isotope fractionation during the precipitation of calcium carbonate. Earth Planet. Sci. Lett. 8, 363 - 371.

Epstein, S., Bushsbaum, R., Lowenstam, H.A., Urey, H.C., 1953. Revised carbonate-water isotopic temperature scale. Geological Society of America Bulletin 64, 417-426.

Fairbanks, R.C., 1989. A 17,000 year glacio-eustatic sea level record: influence of glacial melting rates on the Younger Dryas event and deep ocean circulation. Nature 342, 637-642.

Fenton, M., Geiselhart, S., Rohling, E.J., 2000. Aplanktonic zones in the Red Sea. Mar. Micropaleontol. 40, 277-294.

Funk, J.A., von Dobeneck, T., Wagner, T., Kasten, S., 2003. Late Quaternary Sedimentation and Early Diagenesis in the Equatorial Atlantic Ocean: Patterns, Trends, and Processes Deduced from Rock Magnetic and Geochemical Records. In: The South Atlantic in the Late Quaternary: Reconstruction of Material Budget and Current Systems (Eds. Wefer G., Mulitza S., Ratmeyer V.), Spriner Verlag, Berlin, 461-497.

Ganssen, G., Kroon, D., 1991. Evidence for Red Sea surface circulation from oxygen isotopes of modern surface waters and planktonic foraminiferal tests. Paleoceanography 6, 73-82.

Garbe-Schönberg C.-D., 1993. Simultaneous determination of 37 trace elements in 28 international rock standards by ICP-MS. Geostandards Newsletter 17, 81-93.

Haase, K.M., Mühe, R., Stoffers, P., 2000. Magmatism during extension of the lithosphere: geochemical constraints from lavas of the Shaban Deep, northern Red Sea. Chem. Geol. 166, 225-239.

Hartmann, M., Scholten, J.C., Stoffers, P., Wehner, F., 1998 a. Hydrographic structure of brine-filled deeps in the Red Sea – new results from the Shaban, Kebrit, Atlantis II, and Discovery Deep. Mar. Geol. 144, 311-330.

Hartmann, M., Scholten, J.C., Stoffers, P., 1998 b. Hydrographic structure of brine-filled deeps in the Red Sea: correction of Atlantis II Deep temperatures. Mar. Geol. 144, 331-332.

Hemleben, C., Meischner, D., 1989. Isotopic palaeo-oceanography of the central Red Sea. Lecture, III International Congress on Palaeoceanography, Cambridge, 1989, In: Terra Abstracts 1, 7.

Hemleben, C., Roether, W., Stoffers, P., 1996 a. Östliches Mittelmeer, Rotes Meer, Arabisches Meer. RV Meteor-Cruise No.31. Meteor-Berichte 96-4, p. 1-282.

Hemleben, C., Meischner, D., Zahn, R., Almogi-Labin, A., Erlenkeuser, H., Hiller, B., 1996 b. Three hundred eighty thousend year long stable isotope and faunal records from the Red sea: influence of global sea level change on hydrography. Paleoceanography 10, 147-156.

Irwin, H., Curtis, C., Cloeman, M., 1977. Isotope evidence for source of diagenetic carbonates formed during burial of organic-rich sediments. Nature 269, 209-213.

Kastner, M., 1999. Oceanic minerals:Their origin, nature of their environment,and signifinance. Proc. Natl. Acad. Sci. USA 96, 3380-3387.

Keeling, J.D., 1958. The concentration and isotopic abundance of carbon dioxide in rural areas. Geochim. Cosmochim. Acta 13, 322-334.

Kelts, K.R., McKenzie, J.R., 1982. Diagenetic dolomite formation in Quaternary anoxic diatomaceous muds of Deep Sea Drilling Project Leg 64, Gulf of California. In: J.R. Curray and D.G. Moore (Editors), Init. Reports DSDP, pp. 553-569.

Killingley, J.S., 1983. Effects of diagenetic recrystallization on 18O/16O values of deep-sea sediments. Nature 301, 594-597.

Kwiecińska, B., Petersen, H.I. 2004. Graphite, semi-graphite, natural coke, and natural char classification – ICCP system. Internatinal Journal of Coal Geology 57, 99-116.

Lamy, F., Arz, H.W., Bond, G.C., Bahr, A., Pätzold J., 2006. Multicentennial-scale hydrological changes in the Black Sea and northern Red Sea during the Holocene and the Arctic/North Atlantic Oscillation. Paleoceanography 21, PA 1008, doi: 10.1029/2005PA001184.

Legge, H.L., Mutterlose, J., Arz, H.W., 2006. Climatic changes in the northern Red Sea during the last 22,000 years as recorded by calcareous nannofossils. Paleoceanography 21, PA 1003, doi:10.1029/2005PA001142.

Locke, S.M., Thunell, R.C., 1987. Paleoceanographic record of the glacial-interglacial cycle in the Red Sea and Gulf of Aden. Paleogeogr. Paleoclimatol. Paleoecol. 64, 163-187.

Manheim, F.T., 1974. Red Sea geochemistry. Initial Reports of the Deep Sea Drilling Project 23, 975-998.

Martinez, F., Cochran, J.R., 1988. Structure and tectonics of the northern Red Sea : catching a continental margin between rifting and drifting. Tectonophysics 150, 1-32.

McLennan, S.M., Murray, R. 1999. Geochemistry of sediments. In: Encyclopedia of Geochemistry (Eds. Marshall C.P., Fairbridge, R.W.), Kluwer Academic Publishers, London, 282-292.

Miller, A.R., Densmore, C.D, Degens, E.T, Hathaway, J.C, Manheim, F.T, McFarlin, P.F, Pocklington, R., Jokela, A., 1966. Hot brines and recent iron deposits in deeps of the Red Sea. Geochimica et Cosmochimica Acta 30, 341-359.

Morcos, S.A., 1970. Physical and Chemical Oceanography of the Red Sea. Oceanogr. Mar. Biol. Annu. Rev. 8, 73-202.

Morse, J.W., 2003. Formation and Diagenesis of Carbonate Sediments. In: Treatise on Geochemistry – The Ocean and Marine Geochemistry. Vol. 7 (Ed. Mackenzie F.T.), Elsevier Ltd., Oxford, 67-85.

Mulitza, S., Donner, B., Fischer, G., Paul, A., Pätzold, J., Rühlemann, C., Segl, M., 2004. The South Atlantic Oxygen Isotope Record of Planktic Foraminifera. In: The South Atlantic in the Late Quaternary: Reconstruction of Material Budget and Current Systems (Eds. Wefer G., Mulitza S., Ratmeyer V.), Spriner Verlag, Berlin, 121-142.

Nadeau, M.J., Grootes, P.M., Schleicher, M., Hasselberg, P., Rieck, A., Bitterling, M., 1998. Sample throughput and data quality at the Leibniz-Labor AMS facility. Radiocarbon 40, 239-245.

Olgun, N. (2007) Heat affected foraminiferal alteration in the Shaban Deep, Northern Red Sea. MSc thesis, Kiel University, p. 87.

Pätzold, J., Moammar, M., Al Farawati, R., Al Hazmi, Y.M.M., Al Otibi, A., Antunes, A., Arz, H.W., Berger, J., Botz, R. Donner, B., Ehrhardt, A., Garbe-Schönberg, C.-D., Ghandourah, M., Hübscher, C., Kahl, G., Klann, M., Klauke, S., Klitzke, U., Legge, H.L., Lichowski, F., Schewe, F., Schmidt, M., Schmitt, M., Seeberg-Elverfeldt, I., Truscheit, T., 2003. Black Sea – Mediterranean – Red Sea, Part 3, Cruise No. 52, Leg 3, METEOR-Report 03-2, Leitstelle Meteor, Institut für Meereskunde der Universität Hamburg, Germany, 59 pages.

Pisciotto, K.A., Mahoney, J.J., 1981. Isotope survey of diagenetic carbonates, Deep Sea Drilling Project Leg 63. In: R.S. Yeats and B.U. Haq (Editors), Initial Reports of the Deep Sea Drilling Project 63. College Station, TX, pp. 595-609.

Pautot, G., Guennoc, P., Coutelle, A., Lyberis, N., 1984. Discovery of a large brine deep in the northern Red Sea. Nature 310, 133-136.

Pearson, P.N., Ditchfield, P.W., Singano, J., Harcourt-Brown, K.G., Nicholas, C.J., Olsson, R.K., Shackleton, N.J., Hall, M.A., 2001. Warm tropical sea surface temperatures in the Late Cretaceous and Eocene epochs. Nature 413, 481-487.

Scholten, J., Stoffers, P., Garbe –Schönberg, D., Moammar, M., 2000. Hydrothermal Mineralization in the Red Sea. In: Cronan, D.S. (Ed.), Marine Mineral Deposits, pp. 369-395.

Schrag, D.P., DePaolo, D.J., Richter, F.M., 1995. Reconstructing past sea surface temperatures: Correcting for diagenesis of bulk marine carbonate. Geochim. Cosmochim. Acta 59, 2265-2278.

Seeberg-Elverfeldt, I.A., Lange, C.B., Arz, H.W., Pätzold, J., Pike, J., 2004 a. The significance of diatoms in the formation of laminated sediments of the Shaban Deep, Northern Red Sea. Marine Geology 209, 279-301.

Seeberg-Elverfeldt, I.A., Lange, C.B., Pätzold, J., 2004 b. Preservation of siliceous microplankton in surface sediments of the northern Red Sea. Marine Micropaleontology 51, 193-211.

Seeberg-Elverfeldt, I.A., Lange, C.B., Pätzold, J., Kuhnt, G., 2005. Laminae type and possible mechanisms for the formation of laminated sediments in the Shaban Deep, northern Red Sea. Ocean Science 1, 113-126.

Siddall, M., Smeed, D.A., Hemleben, C., Rohling, E.J., Schmelzer, I., Peltier, W.R., 2003. Understanding the Red Sea response to sea level. Earth and Planetary Science Letters 225, 421-434.

Siddall, M., Rohling, E.J., Almogi-Labin, A., Hemleben, C., Meischner, D., Schmelzer, I., Smeed, D.A., 2003. Sea-level fluctuations during the last glacial cycle. Nature 423, 853-858.

Stoffers, P., Botz, R., Scholten, J., 1990. Isotope Geochemistry of Primary and Secondary Carbonate Minerals in the Shaban- Deep (Red Sea). In: Heling, D., Rothe, P., Förster, U., Stoffers, P. (Eds), Sediments and Environmental Geochemistry. Springer Verlag, Berlin, pp. 83-94.

Truesdell, A.H., Hulston, J.R., 1980. Isotopic evidence on environments of geothermal systems. In: Fritz, P., Fontes, J.Ch. (Eds), Handbook of Environmental Isotope Geochemistry, Elsevier Sci. Publ. Co., Amsterdam – Oxford – New York,pp. 179-226.

Stuiver, M., Polach, H.A., 1977.Discussion; reporting of C-14 data. Radiocarbon 19, 355-363.

Taylor, G.H., Teichmüller, M., Davis, A., Diessel, C.F.K., Littke, R., Robert, P., 1998. Organic Petrology. Gebrüder Borntraeger, Berlin. 704 p.

Thunell, R.C., Locke, S.M. and Williams, D.F., 1988. Glacio-eustatic sea-level control on Red Sea salinity. Nature 334, 601-604.

Voggenreiter, W., Hötzl, H., Mechie, J., 1988. Low-angle detachment origin for the Red Sea Rift system. Tectonophysics 150, 51-75.

Werner, F., Lange, K., 1975. A bathymetric survey of the sill area between the Red Sea and the Gulf of Aden. Geol. Jahrbuch D13, 125-130.

Zierenberg, R.A, Shanks, W.C., 1986. Isotopic constraints on the origin of the Atlantis II, Suakin and Valdivia brines, Red Sea. Geochim. Cosmochim. Acta, 50, 2205-2214.

Table captions

Tab. 1: Total carbonate- and organic carbon contents of sediment cores 17009-3 and 17008-1.

Tab. 2: ^{14}C-ages of planktonic foraminifera *G. ruber* analysed by using Accelerated Mass Spectrometry.

Tab. 3: Oxygen and carbon isotope values of sedimentary foraminifera shells (*G. ruber*).

Tab. 4: Stable oxygen and carbon isotope values of foraminifera shells from sediment core 17008-1 (*G. bulloides* and *G. sacculifer*).

Tab. 5: Trace element contents of sediment samples from PC 17008-1 (Shaban Deep, east basin).

Tab. 6: Measured maturity distribution in comparison with the organic fluorescence of liptinitic organic matter and the derived maturity. The vitrinite reflectance values marked in bold represent the measured maturity matching the derived one in the respective sample.

Tab. 7: Micro-petrographic characterisation of sedimentary intervals as derived from measured and derived maturity as well as from the type and quality of dispersed organic and mineral matter encountered in the respective samples.

Tab. 8: Organic geochemical data.

Figure captions

Fig. 1: a) Bathymetric map of the Red Sea where stages of continental rifting and seafloor spreading are indicated (after Cochran. 1983); b) Positions of sediment cores 17008-1 and 17009-3 in the Shaban Deep (east basin); brine-seawater interfaces are indicated by gray lines.

Fig. 2: Sediment sequence, ^{14}C-ages of sediments, organic carbon- and calcium carbonate content of sediment core 17008-1.

Fig. 3: Sediment echosounder line (PARASOUND) from the central volcanic cone of the Shaban Deep crossing the southeastern sub basin. Near the volcano is slumped material most likely originating from the central volcanic cone. The arrow marks the nearest position to the location of core PC 17008-1. The sketch illustrates the slumped sedimentary pattern resolved by the echosounder.

Fig. 4: Sediment sequence, ^{14}C ages of sediments, organic carbon- and calcium carbonate content of sediment core 17009-3.

Fig. 5: Stable carbon isotope data of foraminifera samples (*G. ruber*)

Fig. 6: Oxygen isotope data of foraminifera shells (*G. ruber*) in sediment core 17008-1. $\delta^{18}O$ values of selected *G. bulloides* and *G. sacculifer* samples are also given.

Fig. 7: SEM photographs showing different degrees of foraminiferal shell calcite dissolution and calcite re-precipitation on shell surfaces sampled at various sediment depths in core

17008-1. White scale bars are 100µm (total-sized shell, left side image) and 10µm (shell segment, right side image).

Fig. 8: Trace element composition of bulk sediments from core 17008-1 hosting foraminifera samples (*G. ruber*). Mean values (±min/max) of single elements as calculated from data (Tab. 5) are compared with element concentrations typical of pelagic clay and deep sea carbonate (after McLennan and Murray. 1999).

Fig. 9: EMPA-data of selected foraminifera from sediment core 17008-1. The EMP photographs show no recognizable alteration of a selected foraminifera sample at 2.5-4 cm core depth and intense alteration of the *G. ruber* shell taken at 228-232 cm depth, respectively.

Fig. 10: Characteristic organic petrological features in sediment samples of core 17008-1 (1-11) and 17009-3 (12).

Fig. 11: Results of the organic geochemical investigations of sediment core 17008-1. Total organic carbon (TOC), background fluorescence of OM, Tmax, hopene/hopane ratios, odd-even-predominance (OEP) and C32 αβ S/S+R are given (further discussion see text).

Fig. 12: GC-FID traces of representative aliphatic fractions extracted from sediment core 17008-1 (a: normal background sediment; b: sediment with “oil-type” hydrocarbons).

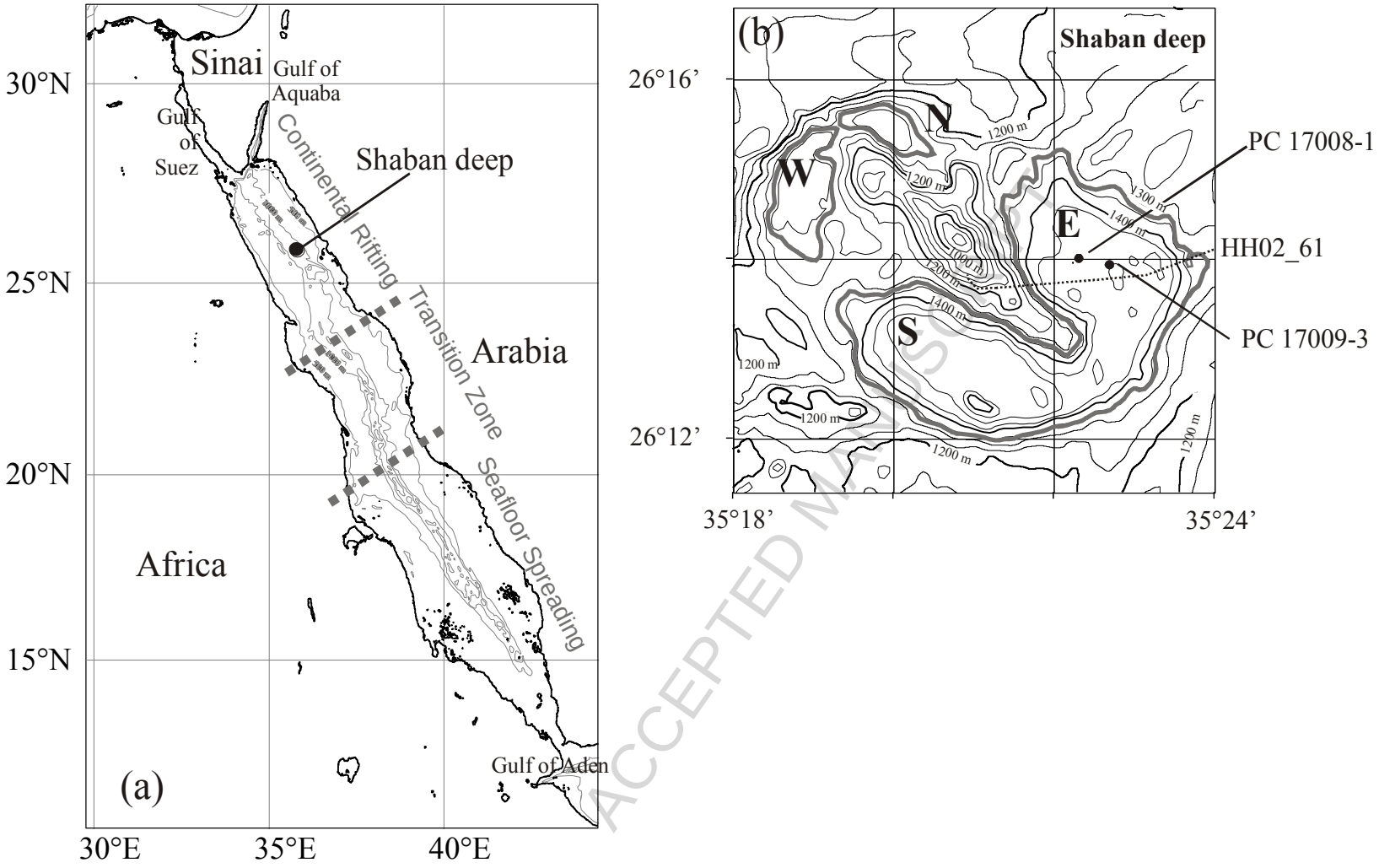

Fig. 1

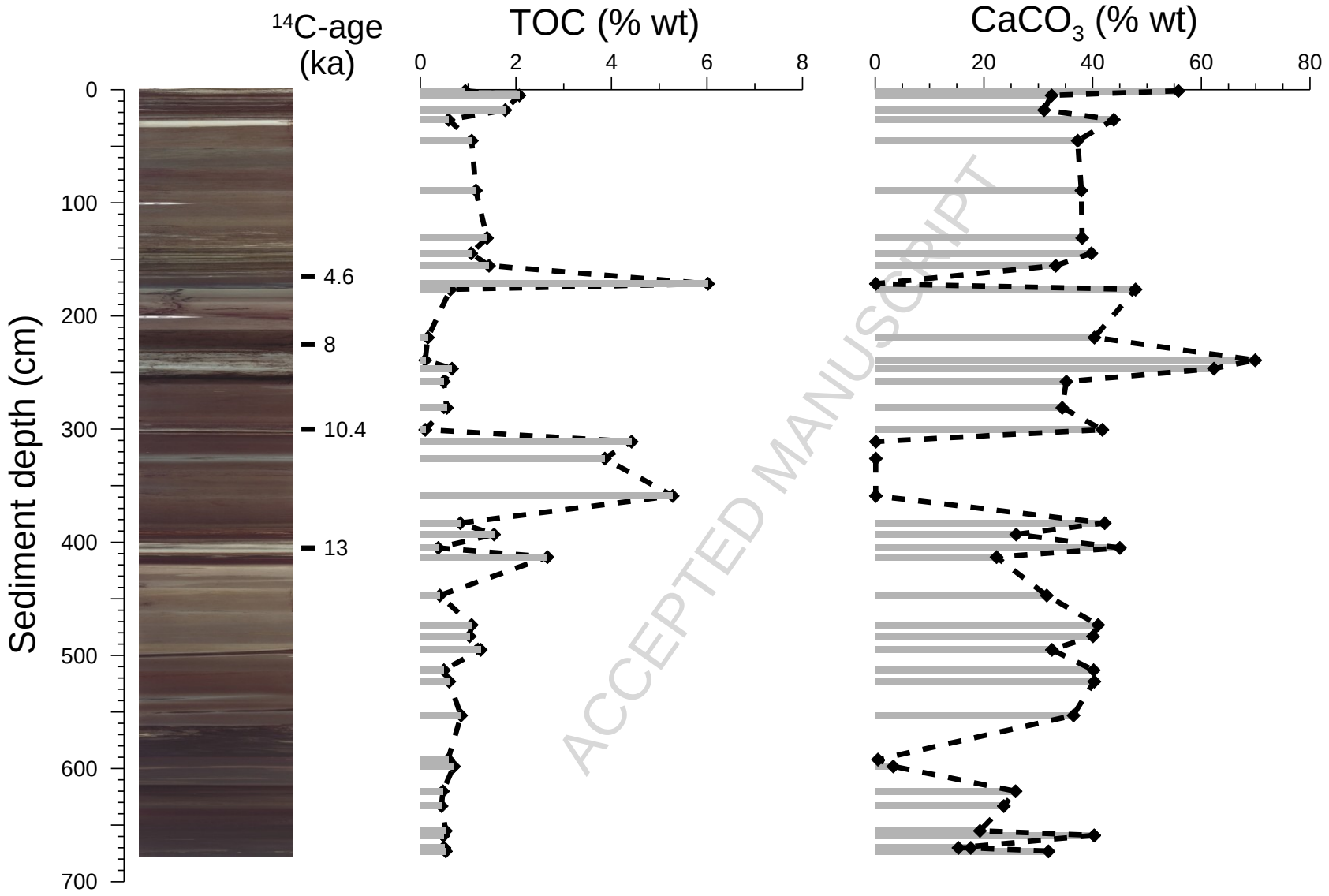

Fig. 2

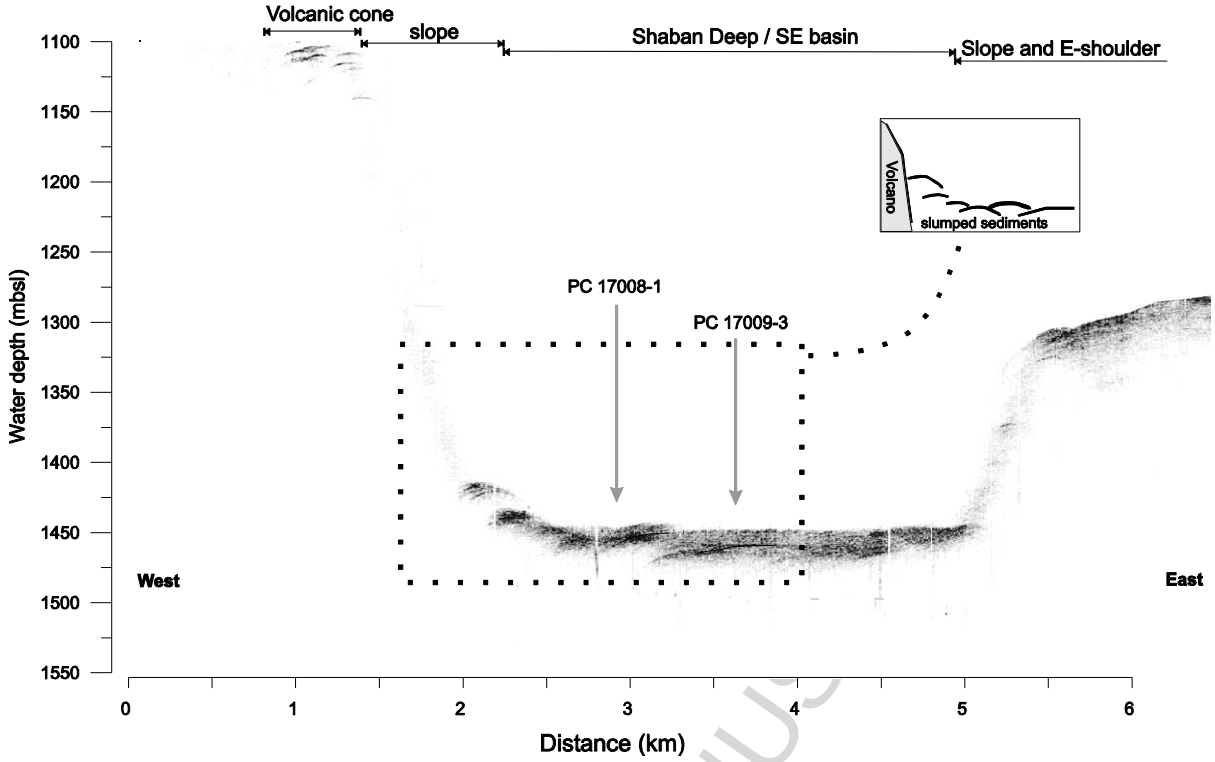

Fig. 3

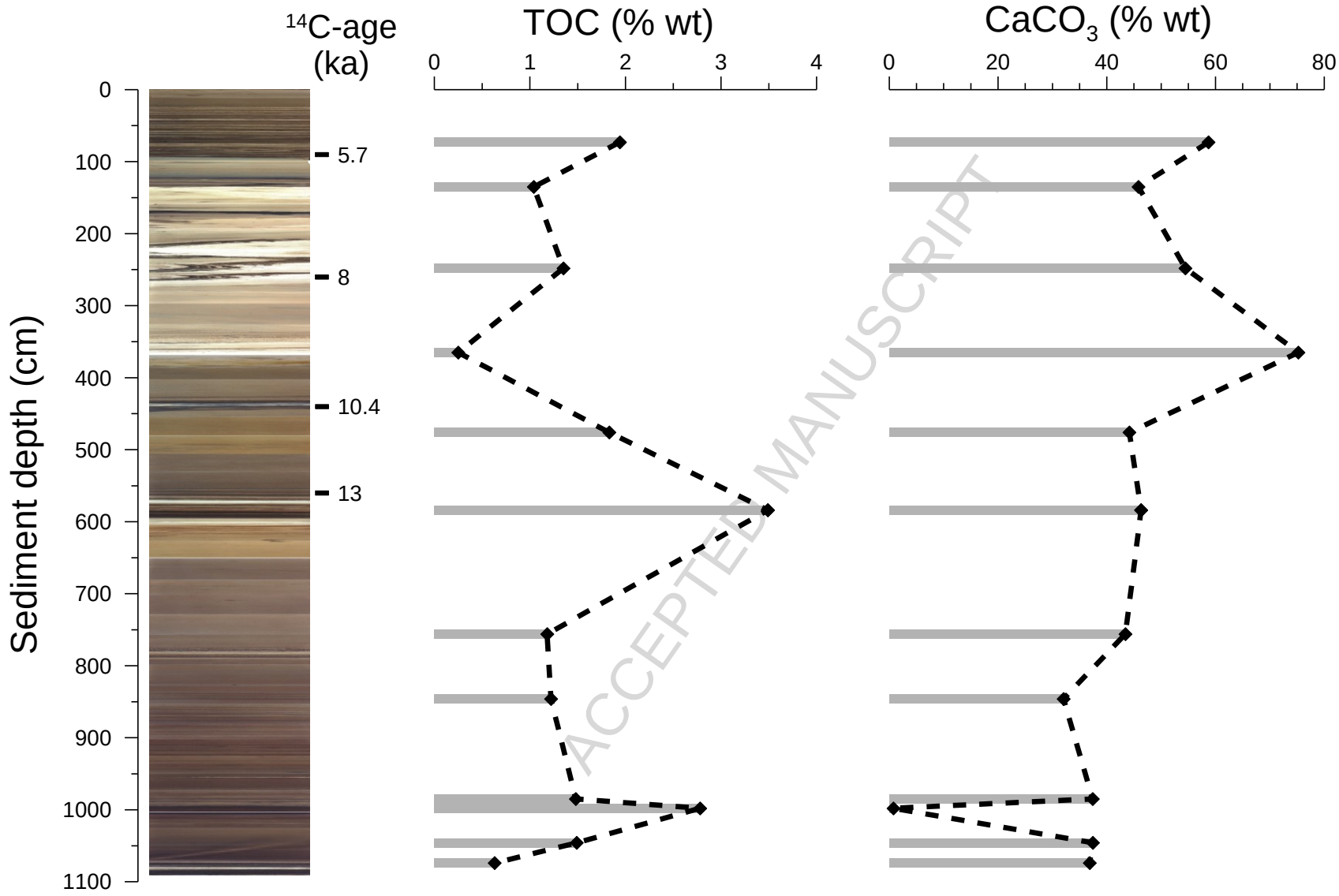

Fig. 4

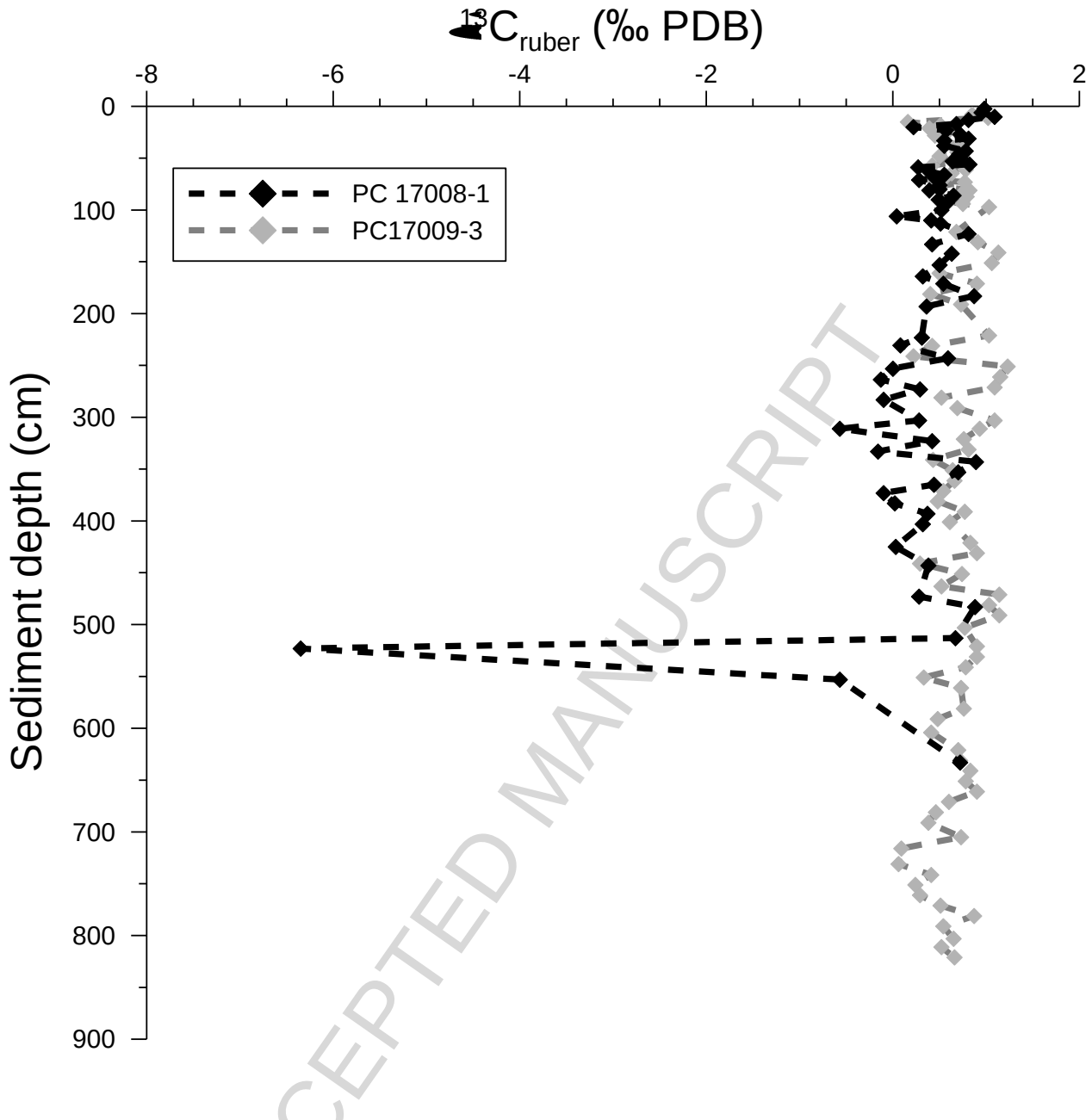

Fig. 5

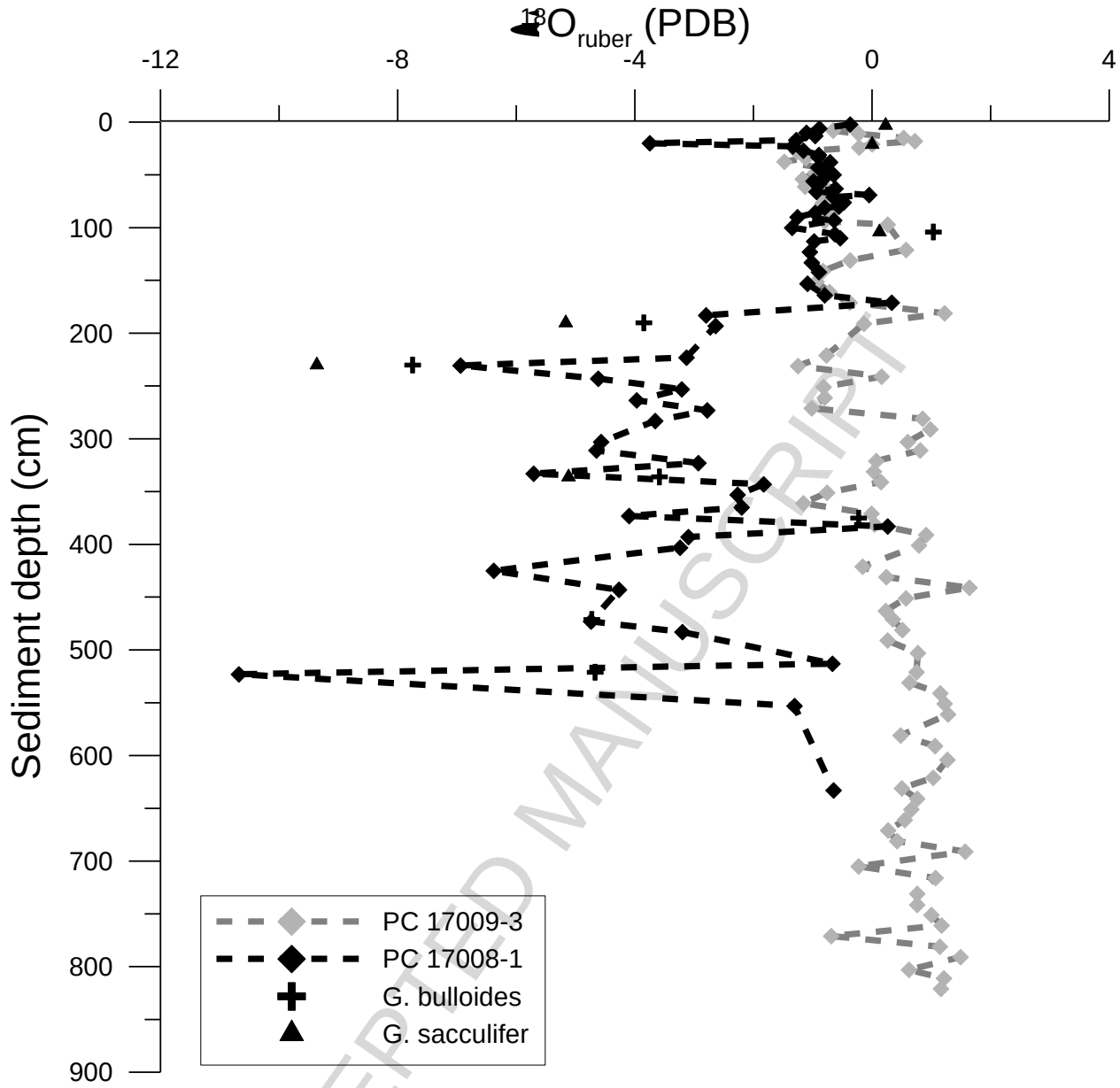

Fig. 6

Depth (cm)	Type	SEM	microscopic observation
2.5-4	*G.sacculifer*	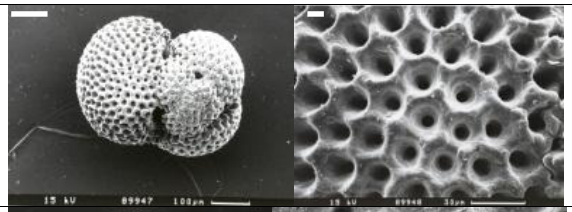	well-preserved unaltered
103-105	*G.ruber*	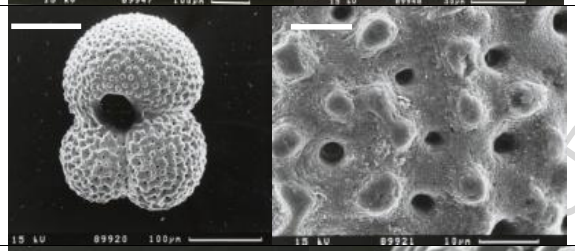	well-preserved unaltered
189-193 228-232 233-236 296-299	*G.ruber*	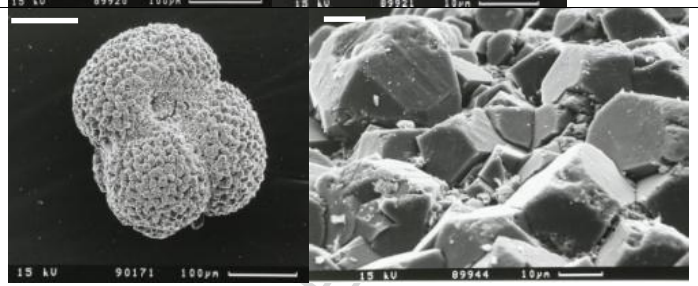	intense alteration euhedral calcitic overgrowth (crystals >10µm) former pores are filled with calcite cement
374-377 380-386	*G. ruber*	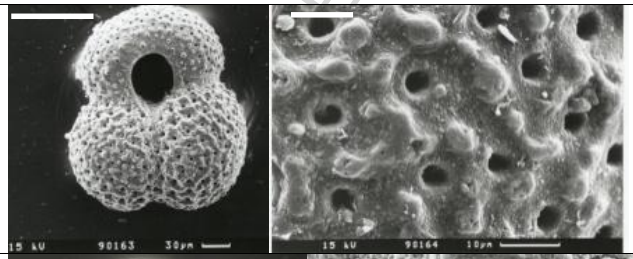	minor dissolution near pores no overgrowth
470-472 508-515 519-526 544-546 550-556	*G. ruber*	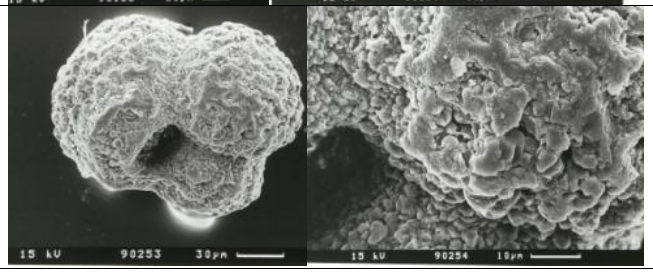	intense alteration intense dissolution anhedral calcitic overgrowth (crystals <2µm)

Figure 07

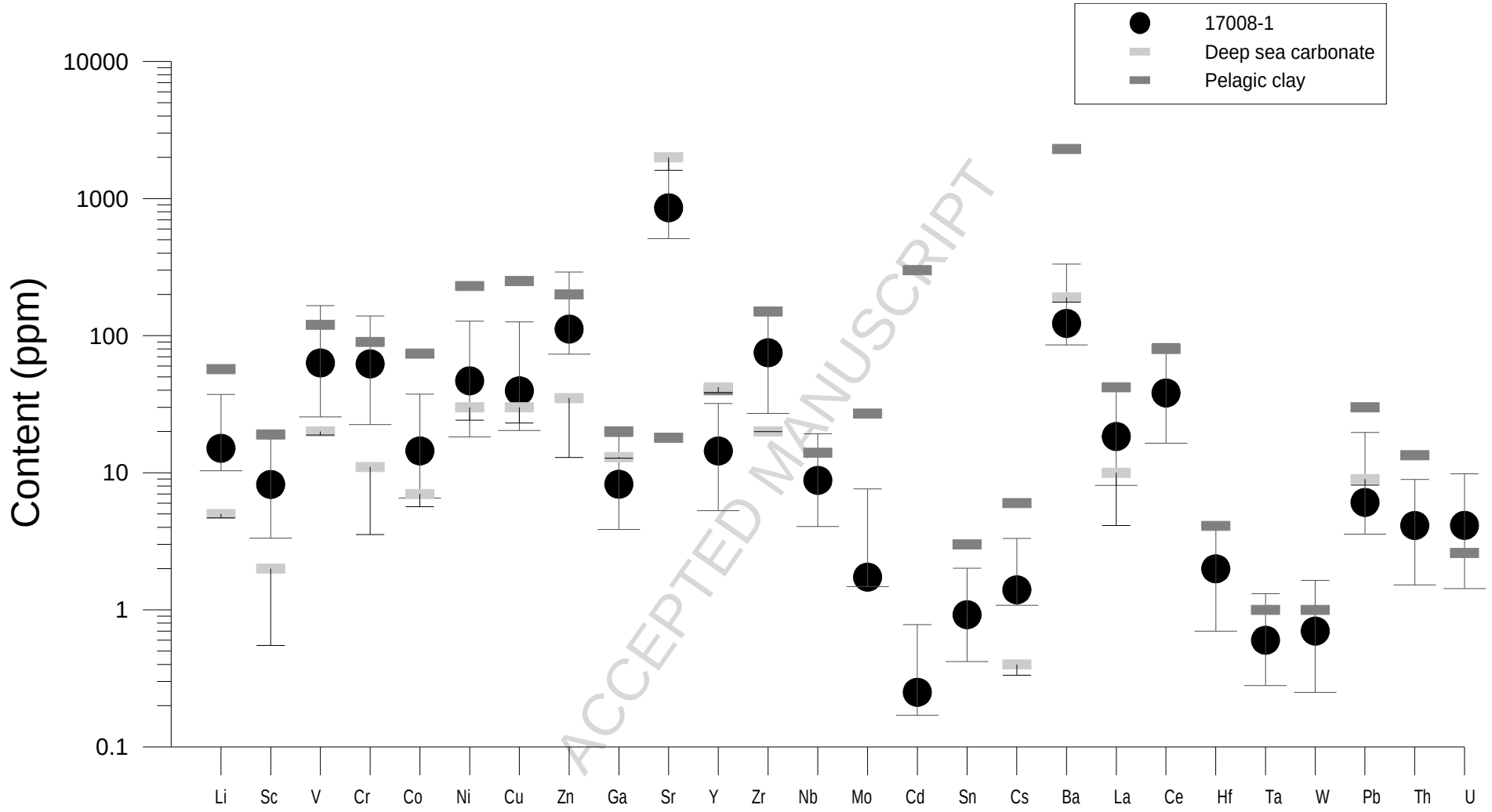

Fig. 8

Depth (cm)	Type	EMP photography	Geochemical data (mean value ± stdv. wt %)
2.5-4	*G.sacculifer* *No recognizable alteration*	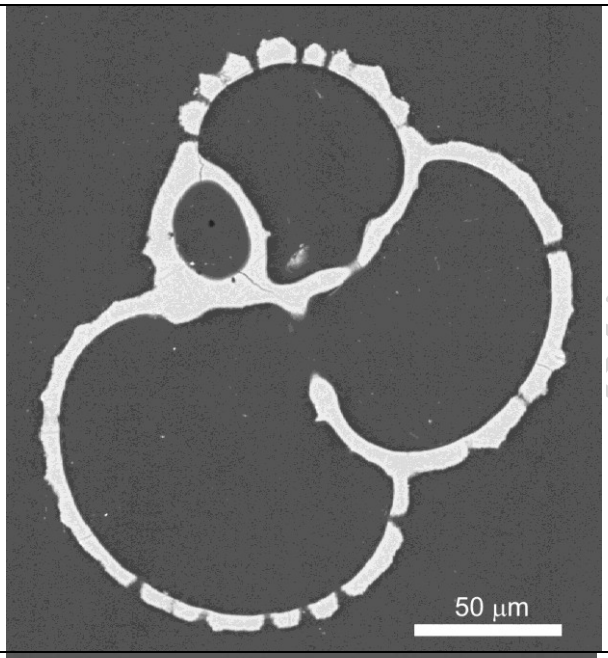	CaO 54.6 ± 0.1 MgO 0.17 ± 0.04 FeO 0.03 ± 0.04 MnO 0.03 ± 0.02 SrO 0.13 ± 0.03 total carbonate 98.2 ± 0.1 n = 27
228-232	*G.ruber* *intense alteration*	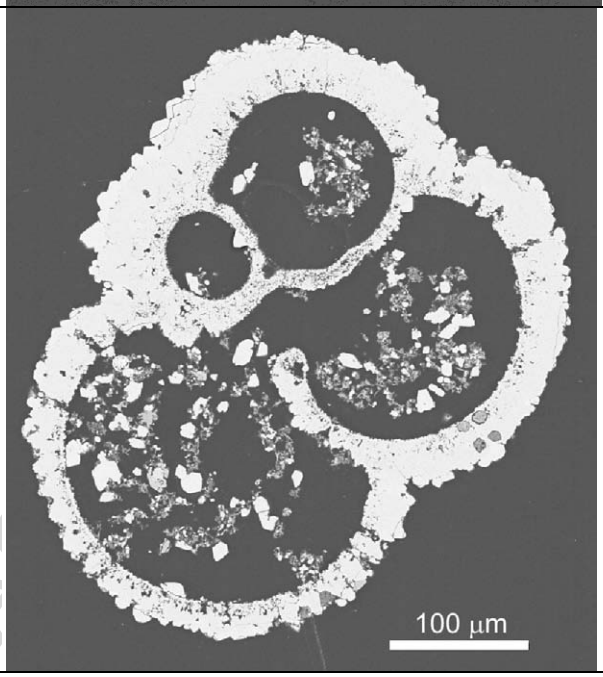	CaO 53 ± 13 MgO 0.28 ± 0.14 FeO 0.04 ± 0.06 MnO 0.24 ± 0.30 SrO 0.11 ± 0.03 total carbonate 96.2 ± 2.4 n = 21

Fig. 9

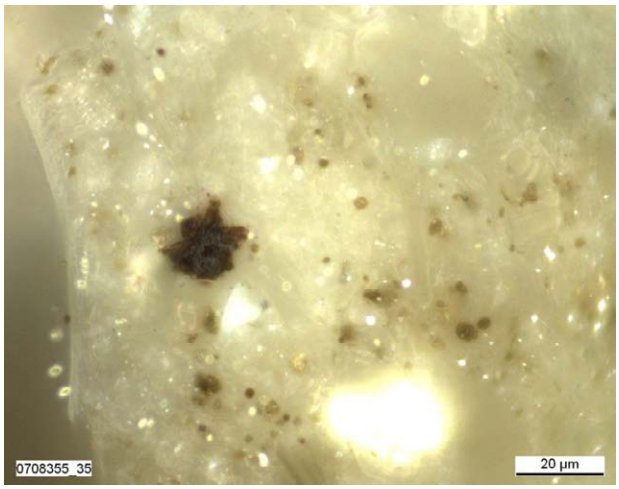

1. Sample 1 – Dark grey porous detrohuminite in white incident light illumination.

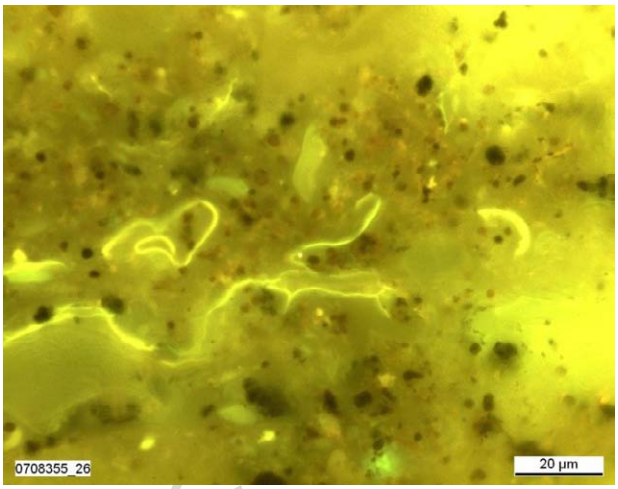

2. Sample 1 – Intensive yellow fluorescent pollen under blue light illumination.

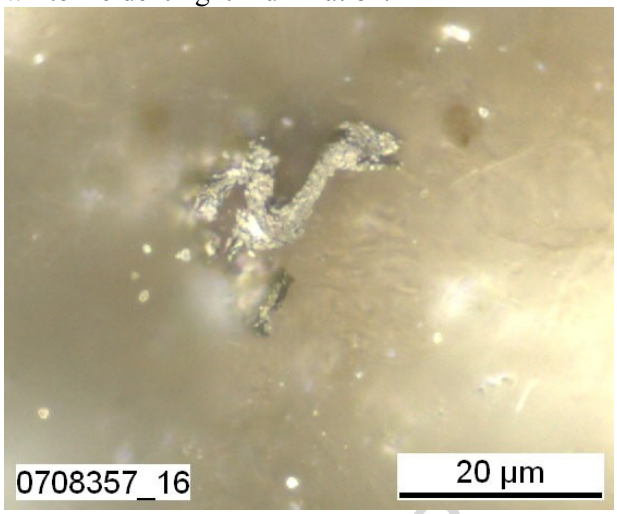

3. Sample 3 – Fein mosaic anisotropy observed in natural coke particle in white incident light illumination.

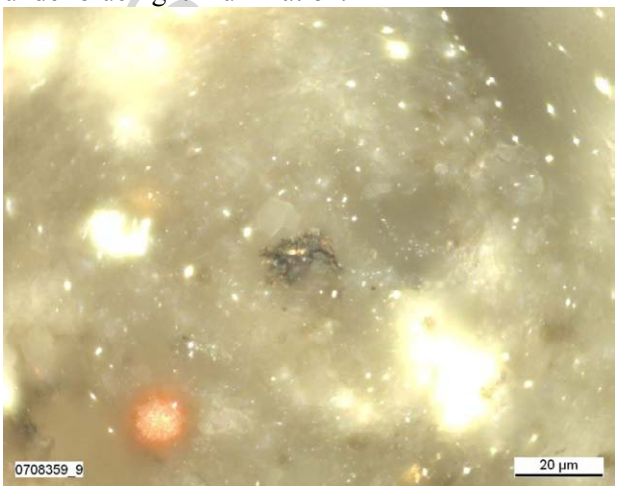

4. Sample 5 – Degraded detrovitrinite particle in white incident light illumination.

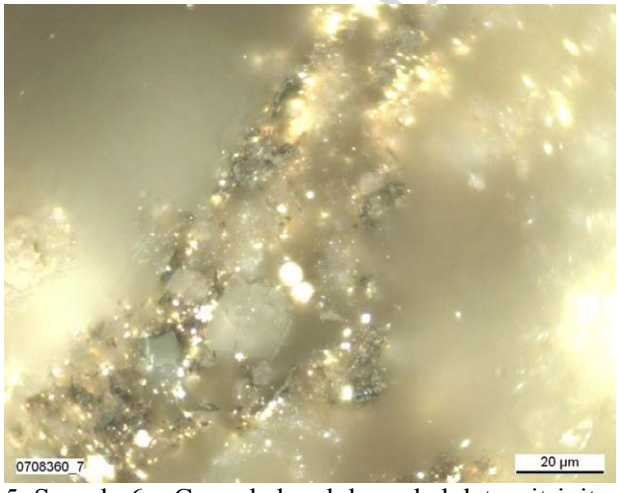

5. Sample 6 – Corroded and degraded detrovitrinite particles in white incident light illumination.

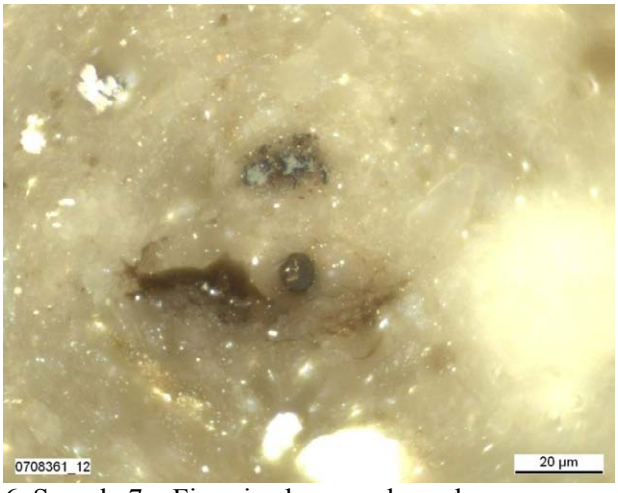

6. Sample 7 – Fine sized grey coloured detrovitrinite together with bituminite of dark brown shade in white incident light illumination.

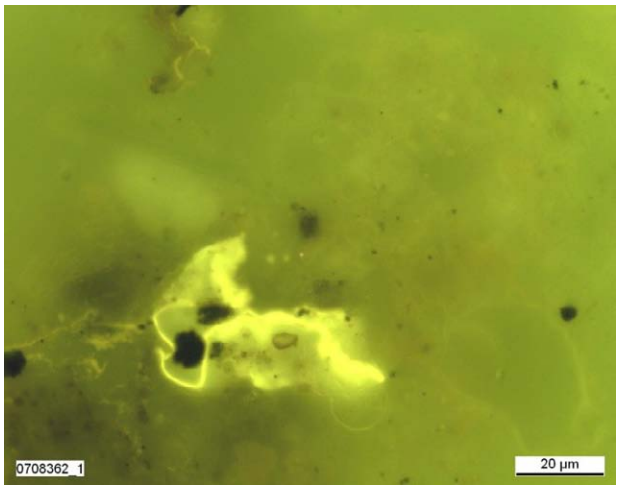

7. Sample 8 – Intensive yellow fluorescent pollen with air sacs under blue light illumination.

8. Sample 9 – Pale yellow fluorescent alginite under blue light illumination.

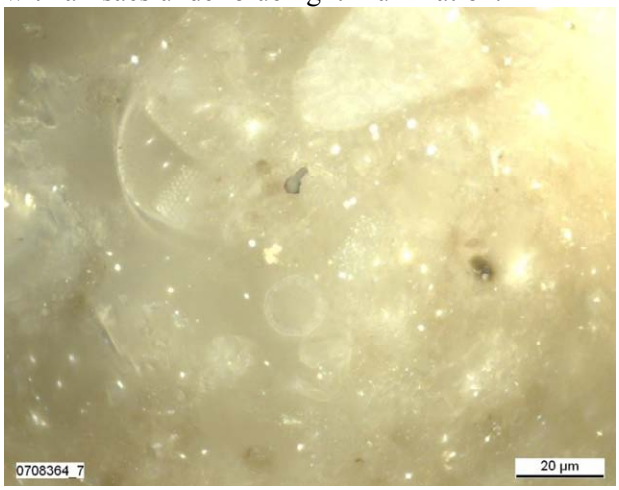

9. Sample 10 – Detrovitrinite white incident light illumination.

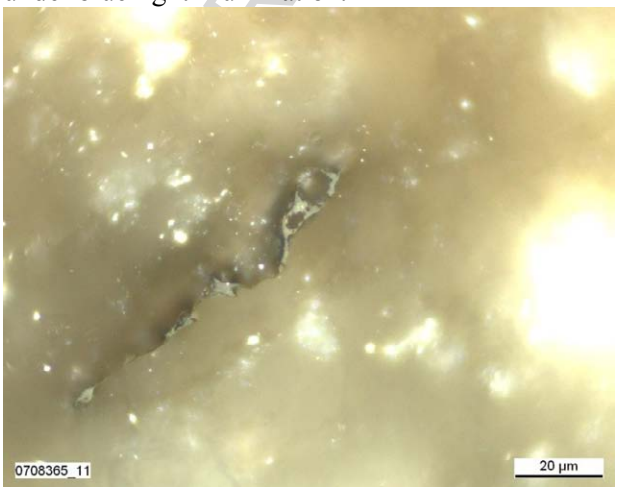

10. Sample 11 – Degraded and porous terrigeneous organic matter in white incident light illumination

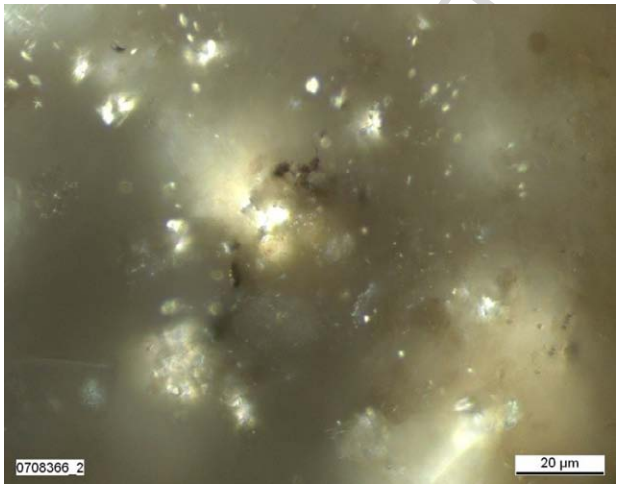

11. Sample 12 – Very fine sized detrohuminite in white incident light illumination.

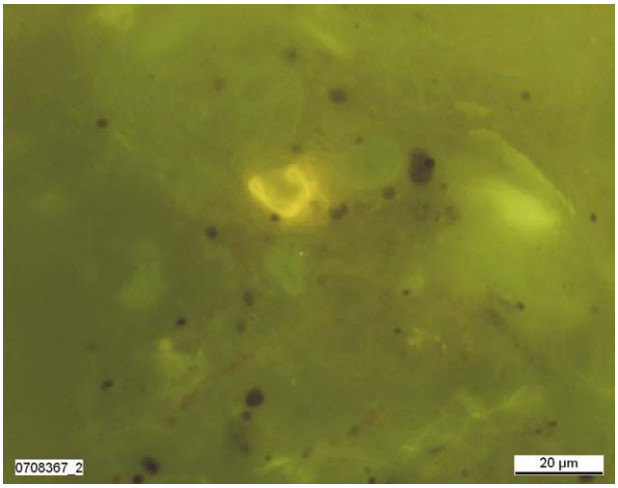

12. Sample 13 – Yellow fluorescent sporomorph under blue light illumination.

Fig. 10

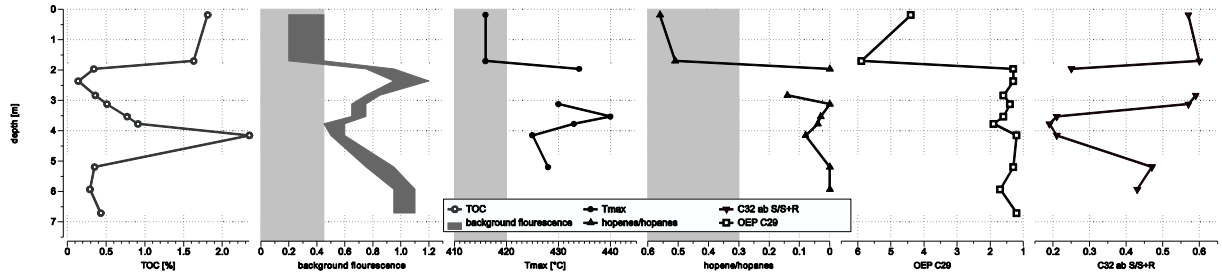

Fig. 11

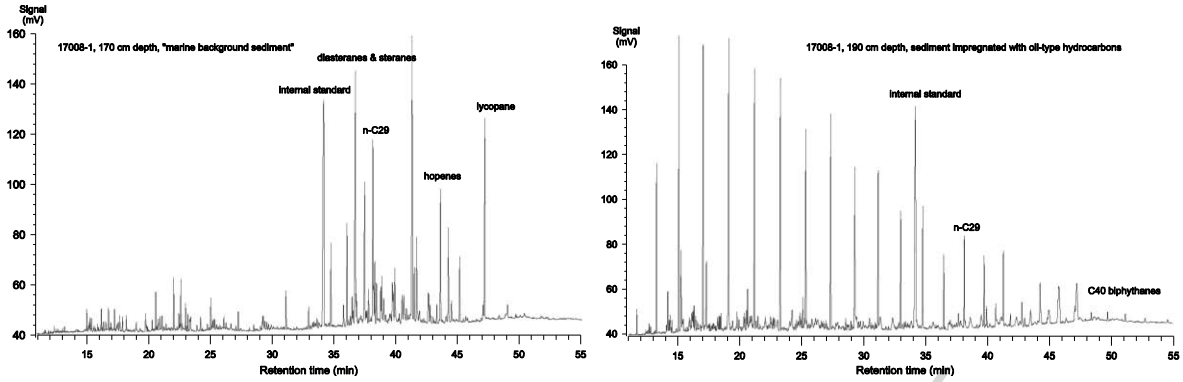

Fig. 12

Tab. 1

Sediment depth (cm)	$CaCO_3$ (wt %)	TOC (wt %)
	PC 17009-3	
73	58.69	1.94
135	45.82	1.04
248	54.46	1.35
365	75.23	0.25
476	44.15	1.83
584	46.3	3.49
584	46.3	3.49
756	43.43	1.18
846	32.04	1.22
985	37.41	1.48
998	0.74	2.78
1046	37.43	1.49
1074	36.84	0.63
	PC 17008-1	
1.00	55.75	0.94
5.00	32.43	2.07
18.00	31.05	1.77
26.50	43.87	0.59
45.00	37.24	1.07
89.00	37.92	1.16
131.00	38.07	1.39
144.50	39.76	1.06
155.50	33.18	1.43
171.50	0.10	6.02
176.50	47.88	0.63
219.00	40.32	0.15
239.00	69.89	0.10
246.50	62.31	0.66
258.00	35.14	0.49
281.00	34.39	0.55
300.50	41.77	0.10
311.00	0.10	4.42
326.00	0.10	3.86
359.00	0.10	5.28
383.00	42.21	0.83
393.00	25.91	1.54
405.00	45.00	0.37
413.00	22.30	2.66
447.00	31.53	0.41
473.00	40.99	1.07
483.00	40.04	1.03
495.00	32.49	1.26
513.00	40.18	0.49
523.00	40.28	0.60
553.00	36.45	0.85
592.00	0.49	0.58

598.00	3.29	0.70
620.00	25.80	0.47
633.00	23.64	0.44
655.00	19.25	0.53
659.00	40.27	0.48
659.00	40.27	0.48
670.00	15.30	0.50
670.00	17.54	0.48
673.00	31.85	0.53

Tab. 2

Core No.	**Sediment Depth** (cm)	**^{14}C-age** (ka)
17008-1	165	4.60
	225	8.00
	300	10.40
	405	13.00
17009-3	90	5.70
	260	8.00
	440	10.40
	560	13.00

Tab. 3

Sediment depth (cm)	$\delta^{18}O$ (‰ V-PDB)	$\delta^{13}C$ (‰ V-PDB)
PC 17009-3		
8	-0.66	0.85
11	-0.23	1.02
15	0.53	0.16
18	0.72	0.51
21	0.00	0.39
24	-0.22	0.59
28	-1.27	0.45
34	-1.12	0.57
37.5	-1.48	0.71
44	-0.79	0.69
48	-0.96	0.50
54	-1.17	0.65
57	-0.86	0.42
61	-1.13	0.78
64.5	-0.75	0.63
67.5	-0.90	0.57
71	-0.83	0.43
73	-0.69	0.77
77	-0.84	0.50
81	-0.63	0.82
84	-0.93	0.74
87	-0.77	0.79
91	-0.83	0.54
94	-0.80	0.75
97	0.26	1.03
121	0.57	0.68
131	-0.37	0.91
141	-0.83	1.13
151	-0.94	1.06
161	-0.72	0.50
171	-0.38	0.90
181	1.22	0.40
191	-0.14	0.73
221	-0.77	1.03
231	-1.25	0.42
241	0.16	0.22
251	-0.82	1.23
261	-0.80	1.15
271	-1.02	1.09
281	0.85	0.52
291	0.98	0.69
303	0.60	1.09
311	0.81	0.93
321	0.07	0.76
331	0.03	0.81
341	0.15	0.43

351	-0.76	0.64
361	-1.16	0.66
371	-0.01	0.54
381	0.04	0.48
391	0.91	0.77
401	0.79	0.61
421	-0.16	0.83
431	0.24	0.90
441	1.64	0.29
451	0.57	0.74
463	0.23	0.52
471	0.35	1.14
481	0.51	1.03
491	0.26	1.14
503	0.77	0.77
521	0.75	0.90
531	0.63	0.90
541	1.15	0.78
551	1.22	0.33
561	1.28	0.73
581	0.48	0.76
591	1.06	0.48
604	1.27	0.41
621	1.03	0.70
631	0.50	0.72
641	0.76	0.83
651	0.66	0.78
661	0.55	0.90
671	0.27	0.60
681	0.42	0.46
691	1.57	0.38
705	-0.23	0.73
716	1.07	0.09
731	0.76	0.06
	0.76	0.41
751	1.00	0.24
761	1.17	0.29
771	-0.69	0.51
781	1.14	0.87
791	1.49	0.54
803	0.62	0.65
811	1.21	0.52
821	1.16	0.66
831	1.36	0.63

PC 17008-1

2.25	-0.37	0.98
6	-0.89	0.95
10	-1.11	1.09
13	-0.96	0.81
17	-1.28	0.68

20	-3.75	0.22
23	-1.34	0.57
27	-1.16	0.72
31	-0.90	0.81
33	-0.91	0.55
38	-0.71	0.55
43	-0.91	0.78
46	-0.82	0.71
50	-0.65	0.72
53	-0.81	0.64
56	-0.99	0.82
58.75	-0.90	0.27
63	-0.62	0.39
66	-0.94	0.55
69	-0.05	0.45
71	-0.65	0.28
76	-0.48	0.50
80	-0.56	0.50
81	-0.80	0.39
86	-0.96	0.65
90	-1.26	0.49
93	-0.64	0.58
100	-1.35	0.52
106	-0.63	0.04
110	-0.54	0.41
113	-0.98	0.51
123	-1.05	0.81
133	-1.02	0.42
142	-0.90	0.63
153	-1.09	0.50
164	-0.80	0.32
171	0.33	0.54
183	-2.80	0.87
193	-2.64	0.36
223	-3.13	0.31
230.5	-6.94	0.08
243	-4.62	0.59
253	-3.21	0.00
263.5	-3.97	-0.13
273	-2.78	0.29
283	-3.66	-0.10
303	-4.57	0.28
311	-4.65	-0.57
323	-2.93	0.42
333	-5.71	-0.16
343	-1.83	0.89
353	-2.27	0.70
365	-2.20	0.44
373	-4.10	-0.10
383	0.26	0.02
393	-3.10	0.37

403	-3.24	0.32
425	-6.38	0.03
443	-4.27	0.38
473	-4.74	0.28
483	-3.20	0.88
513	-0.67	0.67
523	-10.68	-6.35
553	-1.31	-0.57
633	-0.65	0.72

Tab. 4

G. bulloides			*G. sacculifer*		
Sediment depth (cm)	**$\delta^{18}O$ (‰)**	**$\delta^{13}C$ (‰)**	**Sediment depth (cm)**	**$\delta^{18}O$ (‰)**	**$\delta^{13}C$ (‰)**
103-105	1.03	-0.81	2.5-4	0.23	2.76
189-192	-3.85	-0.25	20.5-21.5	0.00	2.62
228-232	-7.75	-0.76	103-105	0.12	2.26
335-337	-3.59	-2.71	189-192	-5.17	1.96
375-376	-0.23	-1.25	228-232	-9.37	0.61
470-472	-4.73	-3.18	335-337	-5.12	-0.30
519-523	-4.67	-2.41			

Tab. 5

Sediment depth	Li	Sc	V	Cr	Co	Ni	Cu	Zn	Ga	Sr	Y	Zr	Nb	Mo	Cd	Sn	Sb	Cs	Ba	La	Ce	Pr	Nd	Sm	Eu	Gd	Tb	Dy	Ho	Er	Tm	Yb	Lu	Hf	Ta	W	Tl	Pb	Th	U
(cm)	(ppm)																																						
169-173	20.9	8.23	63.9	65.4	23.0	80.5	86.3	180	8.07	1075	13.45	72.3	8.19	3.73	0.46	0.98	3.59	1.91	210	16.2	34.1	3.98	15.4	3.02	0.67	2.89	0.41	2.33	0.46	1.31	0.19	1.23	0.18	1.88	0.59	0.82	1.01	13.6	4.02	5.63
189-193	16.0	7.89	55.6	61.6	15.7	52.8	67.7	117	8.13	942	14.74	79.1	8.46	0.49	0.33	0.93	1.16	1.43	119	17.6	36.7	4.28	16.5	3.25	0.71	3.11	0.44	2.48	0.49	1.41	0.20	1.32	0.19	2.07	0.57	0.82	0.15	4.51	4.00	3.35
228-232	4.73	4.86	37.7	39.8	12.9	32.9	20.5	44.7	4.39	963	9.11	47.9	4.73	0.25	0.08	0.50	1.40	0.32	37.2	10.3	21.7	2.54	9.89	1.95	0.42	1.88	0.27	1.52	0.30	0.87	0.12	0.82	0.12	1.29	0.32	0.54	0.06	2.50	2.60	2.70
335-337	14.8	10.1	102.4	76.8	21.1	56.7	32.6	173	10.2	1212	17.57	84.7	10.13	2.46	0.25	1.07	8.65	1.66	130	23.3	49.4	5.66	21.7	4.23	0.91	4.01	0.56	3.11	0.60	1.72	0.24	1.58	0.23	2.17	0.68	0.94	0.39	7.70	4.81	5.69
380-386	17.0	7.75	91.1	63.0	19.8	51.4	31.4	107	7.48	1064	14.83	79.9	7.85	5.90	0.53	0.80	5.12	1.47	136	18.5	39.8	4.53	17.4	3.42	0.75	3.26	0.46	2.59	0.50	1.45	0.21	1.37	0.20	2.13	0.53	0.61	0.70	6.13	4.26	5.30
425-427	22.2	8.33	59.1	64.1	10.4	38.1	29.6	143	9.01	622	14.11	77.1	9.74	2.00	0.20	1.01	1.78	1.92	105	18.1	37.3	4.38	16.7	3.27	0.70	3.11	0.44	2.45	0.48	1.36	0.19	1.26	0.18	2.05	0.66	0.70	0.23	7.13	4.32	4.38
512-514	20.2	8.79	58.9	65.7	10.5	40.9	19.2	120	9.26	760	15.12	83.0	10.26	0.50	0.21	1.09	0.66	1.76	119	19.5	40.2	4.71	18.0	3.51	0.76	3.35	0.47	2.64	0.51	1.48	0.21	1.37	0.20	2.21	0.69	0.69	0.16	4.96	4.51	3.47
519-527	18.2	8.96	59.8	66.9	11.7	43.9	38.2	141	9.43	761	15.67	85.9	10.43	0.64	0.25	1.07	0.60	1.78	123	20.2	41.5	4.90	18.8	3.65	0.79	3.48	0.49	2.73	0.54	1.54	0.21	1.42	0.21	2.30	0.71	0.74	0.16	4.97	4.56	3.62
552-554	6.17	9.48	58.4	66.4	11.1	42.2	25.7	52.0	9.19	819	16.07	80.7	10.29	0.51	0.12	0.96	0.75	0.59	108	21.4	42.7	5.00	19.1	3.68	0.81	3.50	0.49	2.77	0.54	1.56	0.21	1.43	0.21	2.15	0.70	0.71	0.10	4.46	4.39	3.48
632-634	10.7	7.63	45.5	52.8	7.9	28.5	44.4	38.2	7.32	346	13.31	59.3	7.79	0.87	0.12	0.81	0.43	1.11	140	18.8	38.1	4.50	17.1	3.27	0.71	3.06	0.43	2.36	0.46	1.29	0.18	1.18	0.17	1.60	0.53	0.45	0.15	4.76	3.76	3.65

Tab. 6

Sample ID	Measured maturity (% Rr)										Organic fluorescence	Derived maturity (% Rr)
PC 17008-1												
1	0.15		0.38								pale green-green	0.2-0.45
2	0.19		0.37		0.63						pale green - green	0.2-0.45
3	0.15	0.26									pale brown-dark brown	0.75-0.95
4	0.10	0.25	0.42	0.52				0.93			dark brown-black	0.95-1.20
5	0.18		0.38								pale brown	0.75-0.85
6		0.27	0.38	0.57			0.82				dark orange-pale brown	0.65-0.75
7	0.18		0.40								dark orange-pale brown	0.65-0.75
8	0.15	0.27		0.55							Intensive yellow-dark yellow	0.45-0.60
9	0.18										yellow-dark yellow	0.50-0.60
10	0.13		0.38	0.57							brown-dark brown	0.75-0.95
11				0.52		0.72	0.87		1.12	1.42	dark brown	0.95-1.10
12					0.68			0.97			dark brown	0.95-1.10
PC 17009-3												
13		0.27			0.63						orange-dark orange	0.55-0.65
14							0.85		1.12		orange-dark orange	0.55-0.65
15		0.25					0.86				orange-dark orange	0.55-0.65

Tab. 7

Sample ID	Depth	Interval	Association of dispersed organic particles: autochthonous detrohuminite or detrovitrinite	Allochthonous detrovitrinite incorporated at a time of deposition	Allochthonous detrovitrinite incorporated at a time of re-sedimentation	Thermally altered	Comments
					PC 17008-1		
1 2	0.13-0.18 1.67-1.70	1	Yes	Yes	Yes		• Correspondence of representative measured and derived maturity giving rise to autochthonous character of detrohuminite • Incorporation of higher mature detrovitrinite indicative of their allochthonous character either at a time of deposition or resedimentation • Lack of thermally altered dispersed organic particles
3 4 5 6 7	1.89-1.96 2.32-2.36 2.80-2.83 3.09-3.12 3.50-3.53	2			Yes	Yes	• A relative sharp change in the measured and derived maturity pointing towards a clear break in the sedimentation • A wide maturity distribution pointing towards an allochthonous character of the entire interval. reworking most probably at a time of resedimentation • Incorporation of lower mature detrohuminites and detrovitrinites indicating a similar source for these particles as for interval 1. • Incorporation of higher mature detrovitrinite • Apparent presence of thermally altered. i.e.. porous. oxidised. degraded dispersed organic particles • Observation of natural coke particles • Presence of extensively oxidised and corroded framboidal pyrite particles
8 9	3.74-3.77 4.12-4.15	3	Yes				• A renewed sharp change in the measured and derived maturity pointing towards anew break in the sedimentation • Correspondence of representative measured and derived maturity giving rise to autochthonous character of detrovitrinite • Lack of higher mature detrovitrinite • Lack of thermally altered dispersed organic particles

Cont. Tab. 7

Sample ID	Depth	Inter-val	Association of dispersed organic particles: autochthonous detrohuminite or detrovitrinite	Allochthonous detrovitrinite incorporated at a time of deposition	Allochthonous detrovitrinite incorporated at a time of resedimentation	Thermally altered	Comments
10 11 12	5.15-5.19 5.90-5.93 6.67-6.71	4			Yes	Yes	• A renewed sharp change in the measured and derived maturity pointing towards a new break in the sedimentation • An extremely wide maturity distribution pointing towards an allochthonous character of the entire interval. most probably at a time of resedimentation • Incorporation of lower mature detrohuminites indicating a similar source as for the above intervals. • Presence of the highest thermal maturity being measured matching the derived maturity and pointing toward an apparent thermal impact upon the dispersed organic matter
					PC 17009-3		
13 14 15	0.69-0.72 1.72-1.75 1.33-1.36	5	Yes		Yes		• Correspondence of representative measured and derived maturity giving rise to autochthonous character of lower mature detrovitrinite • Incorporation of higher mature detrovitrinite distribution pointing towards their allochthonous character. most probably at a time of resedimentation • Incorporation of some reworked natural coke particles indicative of reworking

Tab. 8

Sediment depth (m)	**TOC** (%)	**Tmax** (°C)	**HI**	**C32 ab S/S+R**	**C30en/ab+en**	**OEP C29**
PC 17008-1						
0.18	1.81	416	265	0.57	0.56	4.4
1.7	1.63	416	235	0.60	0.51	5.9
1.96	0.34	434	106	0.25	0.00	1.3
2.36	0.14					1.3
2.83	0.36			0.59	0.14	1.6
3.12	0.51	430	63	0.57	0.00	1.4
3.53	0.77	440	129	0.21	0.03	1.6
3.77	0.91	433	149	0.19	0.04	1.9
4.15	2.35	425	330	0.21	0.08	1.2
5.19	0.35	428	129	0.47	0.00	1.3
5.93	0.29			0.43	0.00	1.7
6.71	0.43					1.2
PC 17009-3						
0.72	1.45	417	243	0.64	0.73	5.6
1.36	0.6			0.29	0.05	5.6
1.75	0.67			0.37	0.15	5.1

- The Shaban Deep in the Red Sea contains heat-altered foraminiferal shells and organic matter.
- Young basalt extrusions in the Shaban Deep are responsible for recrystallisation and maturation effects.
- Indirect age-dating of basalts by the occurrence of redeposited heat-altered sediment components.
- Detection of migrated hydrocarbons in surface sediments of the Deep.

Research highlights